EXCITATION FORCES ON POINT ABSORBERS EXPOSED TO HIGH ORDER NON-LINEAR WAVES

MASTER THESIS

THOMAS HANSEN VIUFF | MORTEN THØTT ANDERSEN

M.SC., CIVIL ENGINEERING | AALBORG UNIVERSITY | 4. SEMESTER | SPRING 2013

AALBORG UNIVERSITY
STUDENT REPORT

Faculty of Engineering and Science
School of Engineering and Science
Sohngårdsholmsvej 57
9000 Aalborg

Title:

Excitation Forces on Point Absorbers Exposed to High Order Non-linear Waves

Project period:

4rd semester, M.Sc. Structural and Civil Engineering, Spring 2013

Thomas Hansen Viuff

Morten Thøtt Andersen

Supervisor:
Morten Mejlhede Kramer

Circulations: 4
Number of pages: 52
Digital appendices on CD
Completed on Monday the 10th of June 2013

Abstract:

Wave energy devices are often located in intermediate or shallow water close to the free water surface where the wave exposure is extreme. The structures typically consist of large thin curved plates, spherical shells, or cylindrical structures which are sensitive to pressure loads. The lack of proper methods to calculate design pressure distributions has led to structural failures such as buckling in the shells in wave energy prototypes. As a step towards understanding the complex loading from high order non-linear waves, this paper presents a practical approach to estimate wave excitation forces accounting for both non-linearity and diffraction effects. The method is validated by laboratory experiments using a hemispherical point absorber with a 6-axis force transducer, but the technique is believed to be applicable for most types of submerged or semi-submerged floating devices.
The applied method is based on calculation of a peak force coefficient defined as experimentally measured forces on the structure divided by forces estimated by the chosen theoretical method. Methods used include an integration of the undisturbed wave pressure over the surface of the structure, corresponding to the Froude-Krylov force, and a numerical solution to linear potential diffraction theory. Since the two methods have mutual limitations in describing higher order waves and diffraction, a combination of the two will be introduced.

Summary in English

The original proposal for this dissertation comes through some of the structural problems experienced by Wavestar regarding the loads on the floating point absorber. Due to prior buckling failures in the float shell, the scope of this dissertation started out being how to obtain a time and spatially dependent pressure coefficient linking undisturbed pressures to real pressures. During the progress of the work, the focus have shifted to a better description of peak excitation forces on the float. This shift is done, basis of the assumption that once a greater understanding of peak forces is achieved, it will later be less complicated to decompose these into pressures since the theoretical methods all contain a pressure distribution. The final form of the dissertation product consists of three parts.

- Part I - The paper "Excitation Forces on Point Absorbers Exposed to High Order Non-linear Waves".
- Part II - An appendix for the conference paper.
- Part III - Two posters explaining research done prior to final formulation of paper.

The paper is written by Thomas H. Viuff and Morten T. Andersen under supervision of Morten M. Kramer and with experimental assistance from Morten M. Jakobsen. It is meant to be able to stand alone, but for clarifying questions the appendix can be used to some extend. The posters have been presented on the INORE 2013 symposium in Pembrokeshire, UK, along with the preliminary results available at the time.

The work in the parts mentioned above all revolve around describing the complex loads from higher order waves on the hemispherical shell by using different methods with mutual limitations and compare these to experimental results. A Froude-Krylov force is obtained by integration of pressures from an undisturbed wave field on a discretized float shell. This approach is able to model the higher order waves and hereby also describe the changing amount of submerged volume of the float, but neglect all contributions from diffraction and reflection. To take these phenomena into account the numerical tool WAMIT is used to solve the linear potential diffraction theory, the trade-off by this is the inability to account for the change in surface elevation. In the paper a practical method of combining these theories is presented. This method applies a coefficient of diffraction to the higher order Froude-Krylov force and the combined results are compared to experimental measurements.

Summary in Danish (Sammendrag)

Den oprindelige ide til specialet var drevet af firmaet Wavestars problemstilling med estimeringen af bølgelaster i forbindelse med det strukturelle design af flyderen. Med et tidligere konstruktionsmæssigt kollaps som følge af en underestimering af bølgelasterne var den oprindelige ide med specialet at finde en tids- og positionsafhængig trykkoefficient som kombinerede uforstyrede potentialteoretiske trykberegninger med den virkelige trykfordeling på flyderskallen. Igennem arbejdet med specialet ændrede projektet retning til at have mere fokus på en praktisk beskrivelse af de maksimale horisontale og vertikale bølgelaster. Overgangen til dette fokus er gjordt ud fra antagelsen om at når en dybere forståelse for de maksimale bølgelasters parameterafhængighed vil det derefter være lettere at opdele kræfterne i trykfordelinger, da de teoretiske metoder allerede medtager tryk fordelingen. Specialets endelige opdeling er som følger.

1. Del I - Artiklen "Excitation Forces on Point Absorbers Exposed to High Order Non-linear Waves"
2. Del II - Appendiks som understøtter artiklen.
3. Del III - To plakater der forklarer status a projektet forinden udarbejdelsen af artiklen.

Artiklen er skrevet af Thomas H. Viuff og Morten T. Andersen under vejledning af Morten M. Kramer og Morten M. Jakobsen har assisteret i laboratoriet. Artiklen burde give fyldestgørende informationer i sig selv, men appendix kan bruges som supplerende info til en hvis grænse. Plakaterne er brugt i forbindelse med en præsentation af projektet i forbindelse med INORE 2013 symposium konference i Pembrokeshire, UK, sammen med de daværende resultater fra projektforløbet.

Arbejdet i afsnittene beskrevet ovenfor omhandler alle beskrivelsen af de komplekse laster fra højere ordens bøljer på en halvkugleformet skal ved at benytte forskellige metoder, som hver især har forskellige ulemper og sammenligne dem med kraftmålinger foretaget i laboratoriet. Froude-Krylov kraften findes ved trykintegration for uforstyrret tryk over den discretiserede flyderskal. Med denne model er det muligt at modelere højere ordens bølger og derved også at beskrive den varierende mængde af neddykket volumen af flyderen. Samtidig undlades bidrag fra diffraktion og reflektion. For at få disse effekter med i beregningerne benyttes det numeriske værktøj WAMIT til at løse den lineære potentialteoretiske diffraktionsteori. Dog med visse fejl, da WAMIT ikke medtager fluktuationer af vandoverfladen. I artiklen præsenteres en praktisk metode til at kombinere disse teorier. Metoden anvender en diffraktionskoefficient sammen med den højere ordens Froude-Krylov kraft og det samlede resultat sammenlignes med målinger foretaget i laboratoriet.

Table of contents

Part I

Paper

Excitation Forces on Point Absorbers Exposed to High Order Non-linear Waves

Thomas H. Viuff*, Morten T. Andersen†, Morten M. Kramer‡ and Morten M. Jakobsen§
Department of Civil Engineering, Aalborg University
Sohngaardsholmsvej 57, 9000 Aalborg, Denmark
*tviuff08@student.aau.dk, †mtan08@student.aau.dk, ‡mmk@civil.aau.dk, §mmj@civil.aau.dk

***Abstract*—Wave energy devices are often located in intermediate or shallow water close to the free water surface where the wave exposure is extreme. The structures typically consist of large thin curved plates, spherical shells, or cylindrical structures which are sensitive to pressure loads. The lack of proper methods to calculate design pressure distributions has led to structural failures such as buckling in the shells in wave energy prototypes.**

As a step towards understanding the complex loading from high order non-linear waves, this paper presents a practical approach to estimate wave excitation forces accounting for both non-linearity and diffraction effects. The method is validated by laboratory experiments using a hemispherical point absorber with a 6-axis force transducer, but the technique is believed to be applicable for most types of submerged or semi-submerged floating devices.

The applied method is based on calculation of a peak force coefficient defined as experimentally measured forces on the structure divided by forces estimated by the chosen theoretical method. Methods used include an integration of the undisturbed wave pressure over the surface of the structure, corresponding to the Froude-Krylov force, and a numerical solution to linear potential diffraction theory. Since the two methods have mutual limitations in describing higher order waves and diffraction, a combination of the two will be introduced.

***Index Terms*—WEC, hemispherical point absorber, wave loads, wave regimes, non-linear diffraction**

I. Introduction

The heaving point absorber of the Wavestar wave energy converter is an extremely exposed structural component. In an effort to optimize and ease the design of these floats, multiple steps have been taken. Wavestar is currently working on the possibilities of increasing durability by using other materials than glass fiber, e.g. high performance concrete. Besides reconsidering the structural design another focal point is to obtain a better understanding of the wave excitation forces on the float shell. These are generally difficult to describe in higher order waves, and even more so when also taking the dynamic behavior of the point absorber controlled by a PTO strategy into account [1].

This paper will present an attempt to describe and verify the wave excitation forces by investigating three different approaches of obtaining these; an integration of undisturbed wave pressure, a numerical solution of linear potential diffraction theory and an investigation of experimental results. The forces will be related by a coefficient, C_m. To eliminate sources of error, the dynamic movement will not be introduced in this stage of the investigation. Instead the float will be fixed with the point of neutral buoyancy at mean water level.

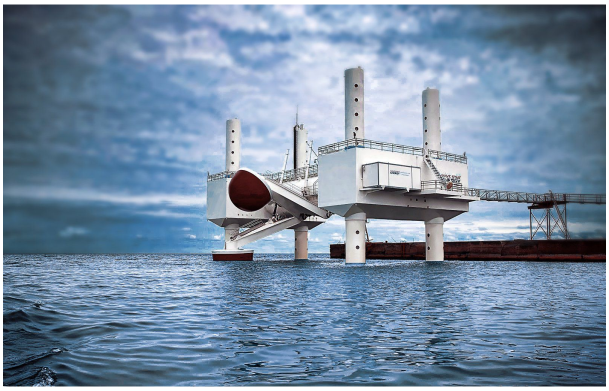

Fig. 1. Wavestar of which the load investigation of the paper concerns [2].

II. Methodology

The three different methods used in this paper all play a part in being able to describe the correct excitation forces on any given body submerged in water. In Table I the different approaches are listed along with the phenomena they do and do not describe. Since drag forces are only obtained through the experiment, there will be an error when determining forces by either Froude-Krylov or linear diffraction theory in a wave regime where drag is not negligible. For regimes where drag can be neglected the aim is to describe the excitation measured in the experiments by either of the two other approaches or a combination of these (diffraction improved Froude-Krylov). To solve the linear diffraction theory the commercial tool WAMIT [3] will be used, and the name WAMIT will figure in the paper when considering the numerical approach and results.

TABLE I
Effects described by methods used in investigation.

	Non-linearity	Diffraction	Drag
Froude-Krylov	X		
Linear diffraction theory		X	
Improved Froude-Krylov	(X)	(X)	
Experiment	X	X	X

III. Methods

The definitions and convention of terms for the considered system are seen in Fig. 2. This convention will be used throughout the different approaches in the paper.

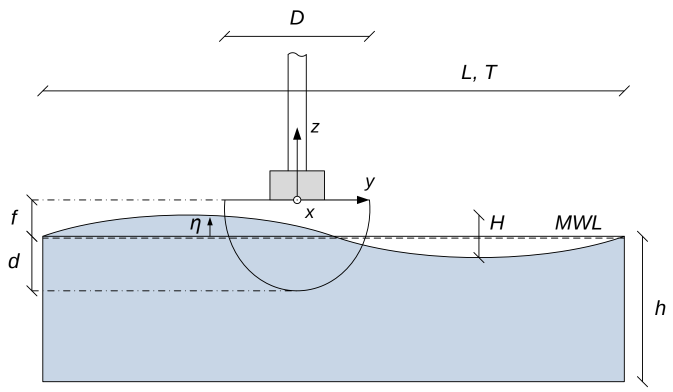

Fig. 2. Paper nomenclature.

A. Undisturbed Pressure Integration

The force from the undisturbed wave pressure field is obtained by an integration over the wetted surface of the body, also known as the Froude-Krylov force [4]. The element model used consists of 538 elements, the diameter is $D = 0.25$ m and the water depth is $h = 0.65$ m, see Fig. 3. The pressure field have been described through Stokes 1st and 5th order, and Dean's stream function theory.

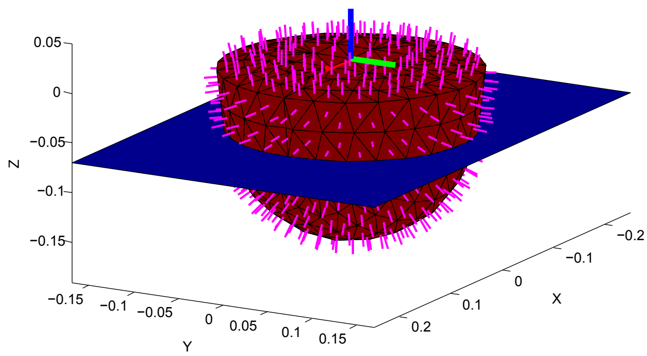

Fig. 3. Element model used for pressure integration. MWL and surface normals are included for illustrative purposes.

To verify the pressure integration scheme a comparison between forces obtained from the analytical MacCamy-Fuchs theory [5], a numerical WAMIT solution and pressure integration of a cylinder of same D and h as the float, is carried out. In Fig. 4 the excitation force amplitudes and phases are shown for all three methods. It is seen that both the direct amplitude/phase output from WAMIT and the amplitude/phase found from integration of pressures from WAMIT match the analytical solution. The integration scheme is considered verified, and will be applied when investigating pressures obtained from undisturbed wave fields.

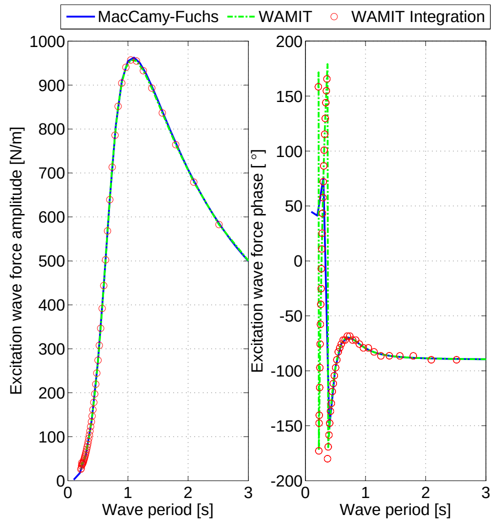

Fig. 4. Verification of pressure integration scheme on cylinder of $D = 0.25$ m and $d = h = 0.65$ m.

The undisturbed pressures from the different wave theories are used in conjunction with the element model of the float seen in Fig. 3, in order to calculate the Froude-Krylov forces. Even though irregular waves can be applied in this approach from superposition of 1st order waves, see Fig. 5, only 1st and 5th order regular waves are used in order to obtain results comparable to the linear results from WAMIT and the regular waves from the experiment.

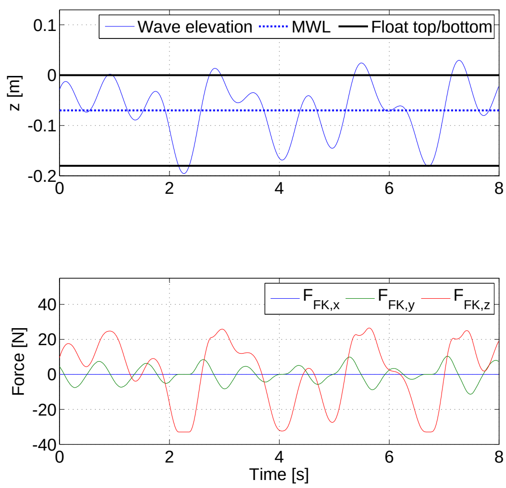

Fig. 5. Froude-Krylov forces from an arbitrary irregular wave on the float shell.

B. Linear Numerical Solution

Unlike the numerical solution obtained from a cylinder to verify the pressure integration scheme, the numerical solution is calculated from the correct float geometry, see Fig 3. Additionally another degree of freedom is also introduced, since now both horizontal and vertical excitations are of interest. The solver for the diffraction theory is limited to linear wave theory and the float geometry above MWL is neglected, i.e. only the draft is considered. This will produce an error compared to the experimental results increasing with wave height.

In Fig. 6 the amplitude and phase of the wave excitation forces on the float can be seen. Excitation amplitude is normalized to wave height, hence the acting force is found by F [N] = A [N/m] $\cdot$ $H/2$ [m]. In the results the expected convergence is clearly visible as $T \rightarrow \infty$, where the horizontal excitation force $F_y \rightarrow 0$ N/m at a -90° phase and $F_z \rightarrow const$ N/m at a 0° phase. This is evidently correct since a infinite period wave will have almost only vertical excitation on the structure with maximum excitation occurring at wave crest, i.e. 0° phase. The horizontal excitation is close to non-existing but still occurs at the theoretical steepest part of the wave at -90° phase.

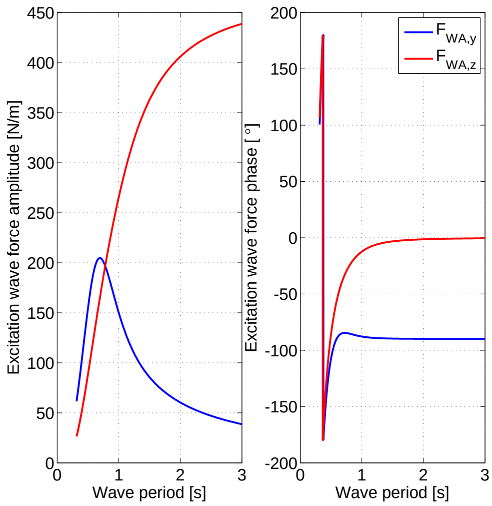

Fig. 6. Frequency response function for float shell obtained from WAMIT.

C. Experimental

In order to validate the calculations using WAMIT or the Froude-Krylov forces from the undisturbed pressure integration, 46 small scale tests with regular waves are carried out on a fixed float shell in the deep water basin at Aalborg University, see Fig. 7. The values and ranges of the experiment are listed in Table II.

The setup used in the experiments can be seen in Fig. 8. The float is placed and fixed at position *F2*. The wave elevation is obtained from wave gauge *WG13* due to its position in phase with the float. The distance from *F2* to *WG13* also helps minimize the error of measuring waves diffracted and reflected by the float.

The test data is filtered and a zero-down-crossing analysis is performed on the measurements from WG13 as shown in Fig. 9. Though the beach at the end of the deep water basin absorbs most of the incoming waves, see Fig. 8, there is still some disturbance from reflected waves. By only including the first seconds of the tests in the experimental analysis, the disturbance from the reflected waves is avoided.

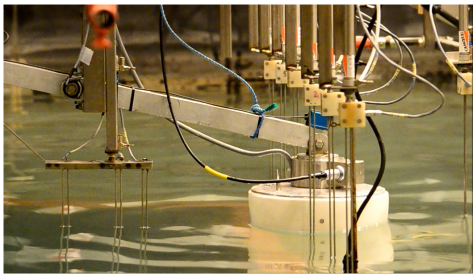

(a) Wave propagation direction from left to right.

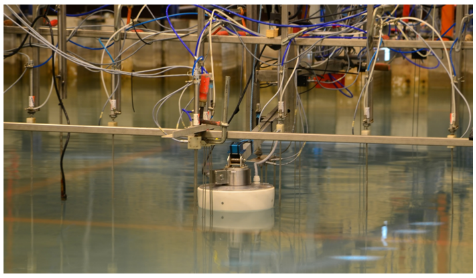

(b) Wave propagation direction towards the camera.

Fig. 7. Images from laboratory tests.

TABLE II
VALUE RANGES OF EXPERIMENT CARRIED OUT IN THE DEEP WATER BASIN.

T [s]	H [m]	h [m]	D [m]	f [m]	d [m]
0.7-2.0	0.01-0.24	0.65	0.25	0.07	0.11

From the zero-down-crossing analysis the actual H and T used in the experiments are found. The wave height and wave period from all tests are listed in Fig.10 to give an idea of which theories are applicable for the different tests.

The forces acting on the float shell in the experiment are

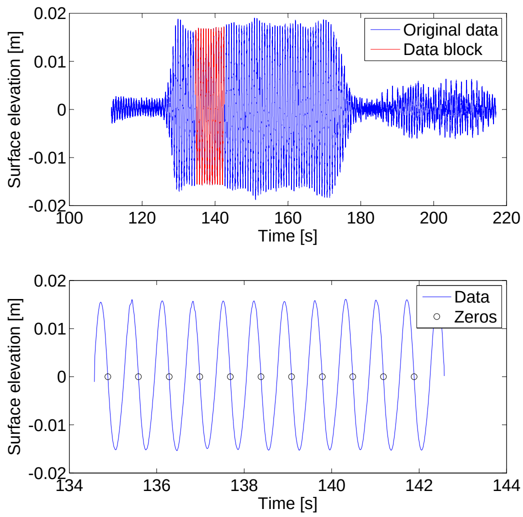

Fig. 9. Data measurements and following zero-down-crossing analysis carried out on test no. 2.

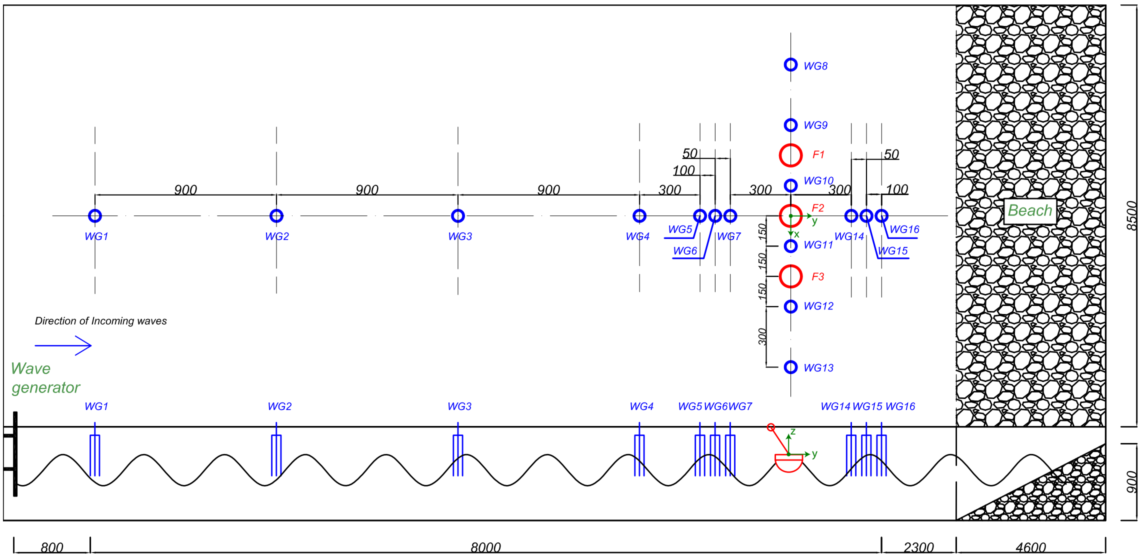

Fig. 8. Setup of equipment in the deep water wave basin.

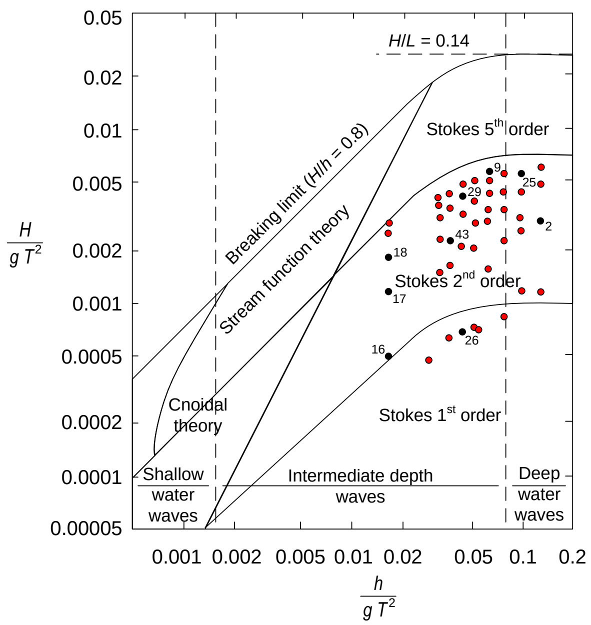

Fig. 10. Theory application overview of the 46 experimental tests. The 9 tests of interest are marked with another color.

measured with a 6-axis force transducer on top of the float measuring forces acting in all 6 degrees of freedom, see Fig. 2.

In order to find trends related to wave height and period, 9 tests are taken out with an approximately even distribution of both wave height and period. These are illustrated on a 3x3 matrix with increasing wave height on the first dimension and increasing wave period on the second dimension. The chosen data are listed in Table III.

The 3x3 matrix overview is shown in Fig. 11 with the test numbers ordered by wave height and wave period. As an example test no. 29 has index (3,2) and all other tests are referred to in the same manor.

TABLE III
WAVE DATA FROM EXPERIMENTS

Test no. [#]	H [m]	T [s]	s [-]	$\eta_{\max}/H$ Experiment [-]	1. order [-]	5. order [-]
2	0.031	0.700	0.04	0.53	0.50	0.53
9	0.137	0.996	0.09	0.57	0.50	0.57
16	0.029	1.987	0.01	0.53	0.50	0.52
17	0.081	1.993	0.02	0.58	0.50	0.55
18	0.140	1.984	0.03	0.63	0.50	0.58
25	0.086	0.797	0.09	0.59	0.50	0.57
26	0.015	1.199	0.01	0.48	0.50	0.51
29	0.135	1.196	0.06	0.49	0.50	0.56
43	0.078	1.300	0.03	0.51	0.50	0.53

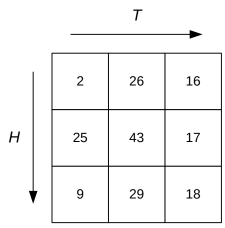

Fig. 11. Concept of test result overview. As a convention, test no. 2 can be referred to as (1,1) and test no. 29 as (3,2).

IV. RESULTS

The three methods are compared using the concept in Fig. 11 as an overview of the changing wave height and wave period. Fig. 12–18 are all using the same configuration. To have an idea of the results a list of parameters are given in the same format, see Fig. 12. The Keulegan-Carpenter number K is calculculated by Equation 1 [6]. The maximum horizontal velocity $U_{\max}$ in Equation 1 is calculated using Stokes 1st

order theory and is the maximum horizontal velocity at the mean water level. The wave length L is calculated from the dispersion relationship [7].

$$K = \frac{U_{\max} T}{D} \tag{1}$$

$K \leq 5$ Limited separation, potential theory usable

$K \geq 5$ Separation occurs, potential theory *not* usable Morrison's Equation should be applied

The fraction $\frac{H}{D}$ is another way of indicating influence of drag or separation. $\frac{D}{L}$ indicates the importance of diffraction and non-linearities are indicated by $s = \frac{H}{L}$ and $\frac{\eta_{\text{max,exp}}}{H}$.

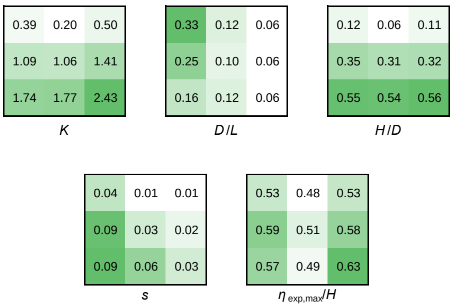

Fig. 12. Trend overview of Keulegan-Carpenter number, normalized wave length, normalized wave height, steepness and $\frac{\eta_{\text{max,exp}}}{H}$. Whiter areas indicate lower numbers within the matrix.

Fig. 12 shows that the Keulegan-Carpenter number increases when H and T increases (drag forces becomes more important) and that the ratio $\frac{D}{L}$ becomes larger for decreasing H and T (diffraction effects become more important). It also explains that s increases for increasing H and decreasing T (non-linear effects become important).

From the wave height and period found by the zero-down-crossing analysis on the measurements from *WG13* in the experiment the regular surface elevation relative to the mean water level for time $0 < t < 2T$ are calculated using Stokes 1$^{\text{st}}$ and 5$^{\text{th}}$ order theory and the results are shown for the 9 different tests in Fig. 13.

For the same time period the vertical and horizontal wave excitation force on the float generated from the regular waves are compared in Fig. 14–15. The two Stoke theories are compared to the measured wave excitation forces from the experiment, both in shape and maximum force.

From Fig. 13 Stokes 1$^{\text{st}}$ order theory becomes less accurate as the wave height increases, which is in accordance with the knowledge of the assumption $\left(\frac{H}{L} << 1\right)$ made in Stokes 1$^{\text{st}}$ order theory. Instead Stokes 5$^{\text{th}}$ order theory is able to describe the surface elevation for all 9 tests, which was expected from the location of the tests in Fig. 10 being within the application area of Stokes 5$^{\text{th}}$ order theory.

The vertical and horizontal wave excitation force time series on the float shell are calculated as Froude-Krylov forces and through WAMIT. Comparing the results in Fig. 14 for the

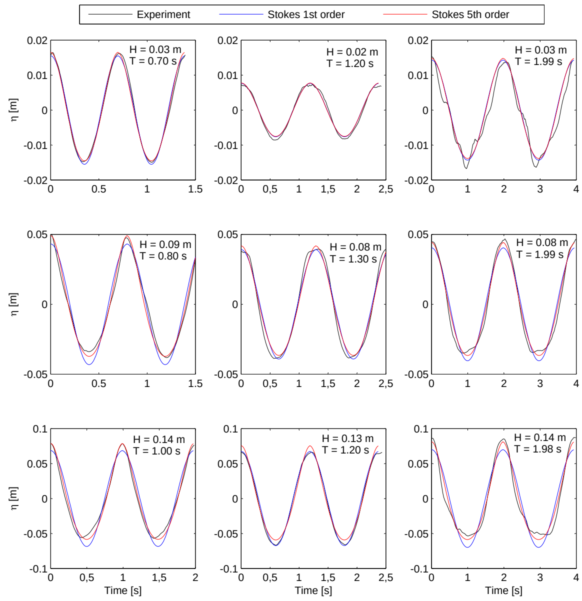

Fig. 13. Comparison of surface elevation between experiment and Stokes 1$^{\text{st}}$ and 5$^{\text{th}}$ order theory.

vertical wave excitation forces with the measurements in the experiment, both results seem to have the same trends as the experiment with the force being proportional to both wave height and wave period. In general Stokes theory overestimates the forces and the error of estimation increases with wave height. The fact that the Froude-Krylov force using Stokes 5$^{\text{th}}$ order theory has the most erroneous results and that WAMIT fits best, indicates that diffraction effects are important for the calculation.

For low wave periods there is a slight phase lag on the results from WAMIT in accordance with Fig. 6 for $T \approx 0.8$ s. Stokes theory does not show the same tendency since it is based on an undisturbed pressure integration.

Comparing the horizontal wave excitation force time series shown in Fig. 15, the results from WAMIT are again showing the best fit, when looking at the maximum forces. The horizontal force measurements from the experiment develops a plateau with increasing wave period, which the Froude-Krylov force mimics, though the amplitude is not of equal size. In general the Froude-Krylov force underestimates the maximum horizontal force. This behavior is not expected since diffraction effects for vertical cylinders makes the horizontal wave excitation forces lower than what would otherwise be found using undisturbed pressure integration [5]. The deviation from the theory could be a result of the geometrical differences.

The WAMIT force time series have the shape of harmonic oscillations and does not show the same trend as the experiment, which can be explained by WAMIT not taking surface elevation into account.

From the results in Fig. 13 and 15 it is seen that Froude-Krylov forces method is better at fitting the shape of the wave excitation time series, because the surface elevation is taken into account when integration the pressures on the float.

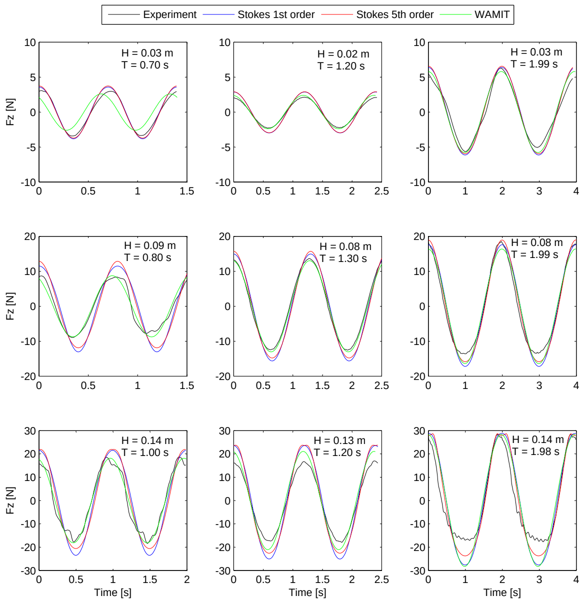

Fig. 14. Comparison of vertical wave excitation force time series between experiment, WAMIT and the Froude-Krylov force using different Stokes theories.

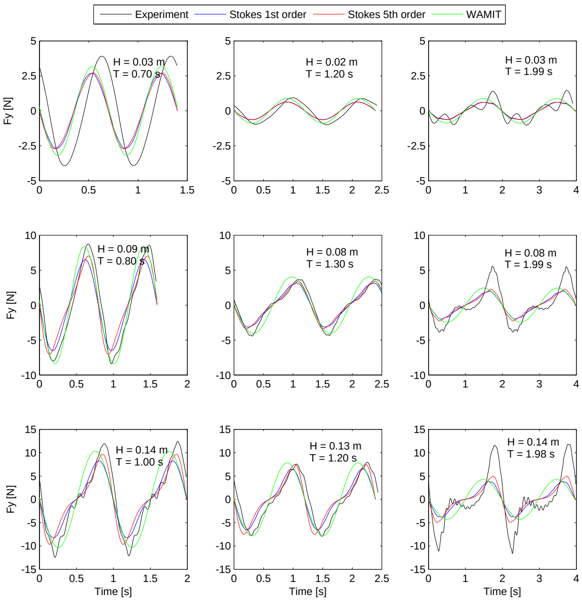

Fig. 15. Comparison of horizontal wave excitation force time series between experiment, WAMIT and the Froude-Krylov force.

The Froude-Krylov force does however lack diffraction effects which WAMIT takes into account. A way of combining the surface elevation and the diffraction effects is by calculating a diffraction coefficient β as a fraction between the maximum forces from WAMIT and the maximum Froude-Krylov forces without surface elevation, see Equations 2.

$$\beta = \frac{F_{\text{WA,max}}}{F_{\text{FK1},\eta\,=\,0,\text{max}}} \tag{2}$$

Multiplying the diffraction coefficient with the Froude-Krylov force based on Stokes 5$^{\text{th}}$ order theory both the diffraction effects and surface elevation are taken into account.

$$F_{\text{FK5d}} = \beta\ F_{\text{FK5}} \tag{3}$$

The result of the calculation is shown in Fig. 16–17.

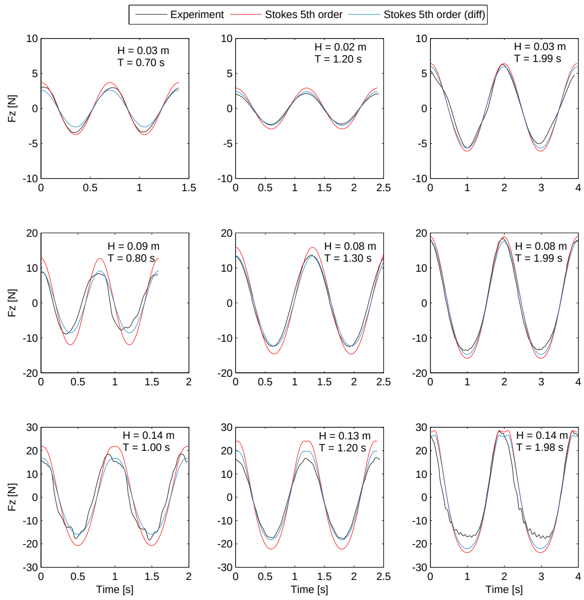

Fig. 16. Comparison of vertical wave excitation force time series between experiment and the improved Froude-Krylov force.

The horizontal wave excitation force time series seems to fit better in shape and size though the improved Froude-Krylov force overestimates the force for test number 43 and 29, shown in Fig. 17 on position (2,2) and (3,2). Looking at Fig. 13 the surface elevation for the same tests are also overestimated, which might explain this deviation from the trend.

Improving the Froude-Krylov force calculation makes the vertical wave excitation forces in Fig. 16 decrease and generally fit better to the actual measurements. It is also observed that the method of including the diffraction using results from WAMIT seems to increase accuracy of the calculations.

The ratio between the maximum forces measured from the experiment and the maximum forces calculated from the different methods are referred to as a peak force coefficient. It is defined as a ratio between the real forces and the estimated forces, see Equation 4. The use of this coefficient is in theory only possible for inertia dominated regions. Regions where inertia forces are dominant are for structural dimensions lower than one fifth of the wave length $\left(\frac{D}{L} \leq 0.2\right)$. This is not the case for (1,1) and (2,1), Fig. 12. For higher numbers of $\frac{D}{L}$ diffraction becomes important and a possible way to overcome this is by including the diffraction coefficient, β.

$$C_m = \frac{F_{\text{exp,max}}}{F_{\text{estimated,max}}} \tag{4}$$

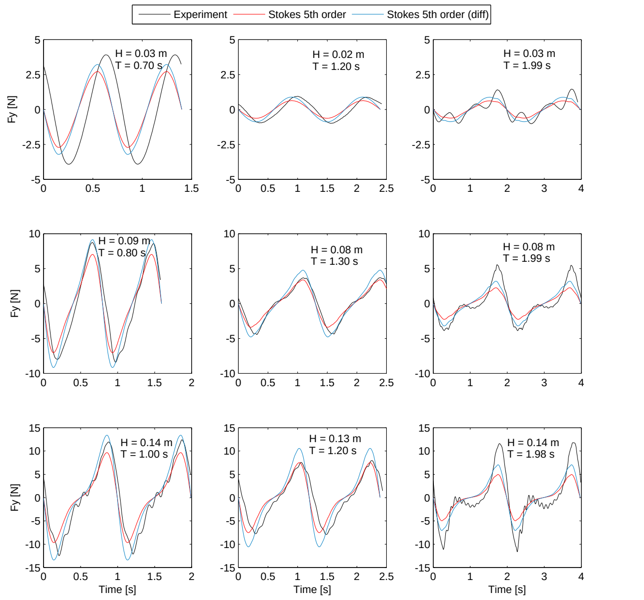

Fig. 17. Comparison of horizontal wave excitation force time series between experiment and the improved Froude-Krylov force.

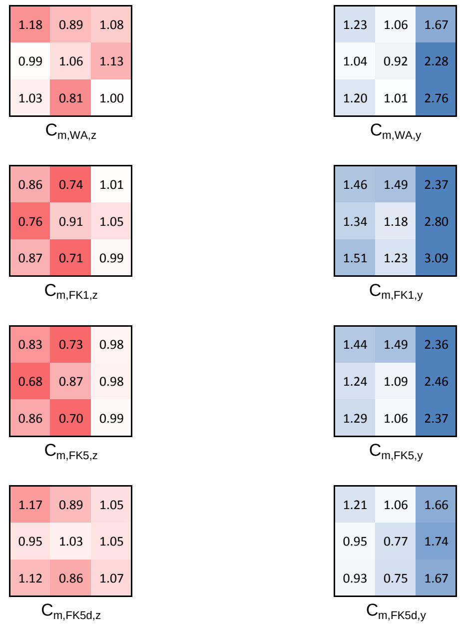

Fig. 18. Trends between C_m from the different methods. Whiter areas indicate a better fit. Different color ranges are applied for F_y than F_z because of the different fit for each direction.

The peak force coefficient, C_m, is calculated for both horizontal and vertical maximum forces and their notations are listed in Table IV.

TABLE IV
GENERAL NOTATION OF PEAK FORCE COEFFICIENTS WITHOUT DIRECTIONAL INDEX.

C_m notation	Method
$C_{m,\text{WA}}$	WAMIT
$C_{m,\text{FK1}}$	Stokes 1st order
$C_{m,\text{FK5}}$	Stokes 5th order
$C_{m,\text{FK5d}}$	Stokes 5th order (diffraction)

The results for each method are shown in Fig. 18, showing a clear improvement in using Stokes 5th order theory with diffraction coefficient, though no clear dependency on K, $\frac{H}{D}$, s or $\frac{\eta_{\text{max,exp}}}{H}$ is to be found, indicating that C_m is depending on more than one parameter. [8] explains the same multi-parameter dependency for horizontal wave excitation forces on vertical cylinders with a dimensional analysis using Stokes 1st order theory. Despite the geometrical differences between the fixed hemispherical point absorber and a fixed vertical cylinder, the test results are put through the same analysis in lack of a better method.

The result from the dimensional analysis for a fixed vertical cylinder is the diagram shown in Fig. 19 (b). The general equation for the dimensional analysis is given in Equation 5 [5]. For large ratios of $\frac{D}{L}$ indicating large diffraction effects, the Reynolds numbers may be omitted. The Keulegan-Carpenter number is usually very low in this case (often in the region of $K < 1$). For small $\frac{D}{L}$ the diffraction effects are negligible and the Keulegan-Carpenter number becomes more important in the dimensional analysis.

$$\frac{F}{\rho g H D^2} = f\left(\frac{d}{L}, \frac{H}{L}, \frac{D}{L}, Re\right) \tag{5}$$

The calculation of the diffraction improved peak force coefficient for Stokes 5th order, $C_{m,\text{FK5d}}$ is carried out for all 36 tests with regular waves, which are not corrupted. The results are shown in Fig. 19 and 20.

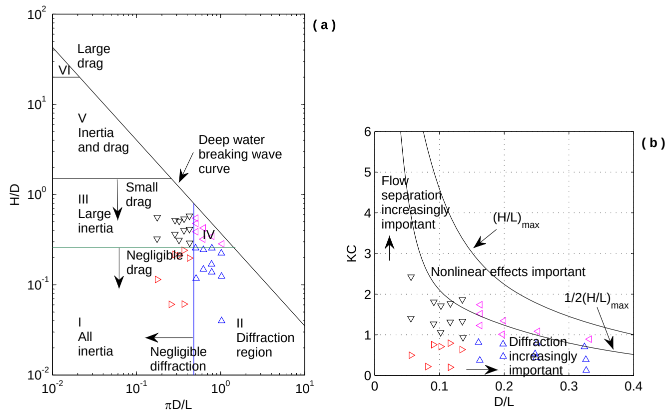

Fig. 19. Test data agains $\frac{D}{L}$ and $\frac{H}{D}$ for $C_{m,\text{FK5d}}$ from Stokes 5th order (diff). (a) Region overview of test data [8]. (b) Test details on wave force regimes [5]. Test results are divided by the defined regions.

A similar diagram is made by [8] shown in Fig. 19 (a) which is used to divide the tests into the defined regions in the graph (I is mostly inertia, II has diffraction effects, III has small drag effects and IV is both influenced by drag and diffraction). The peak force coefficients based on Stokes 5th order theory with and without diffraction effects included are shown in Fig. 20.

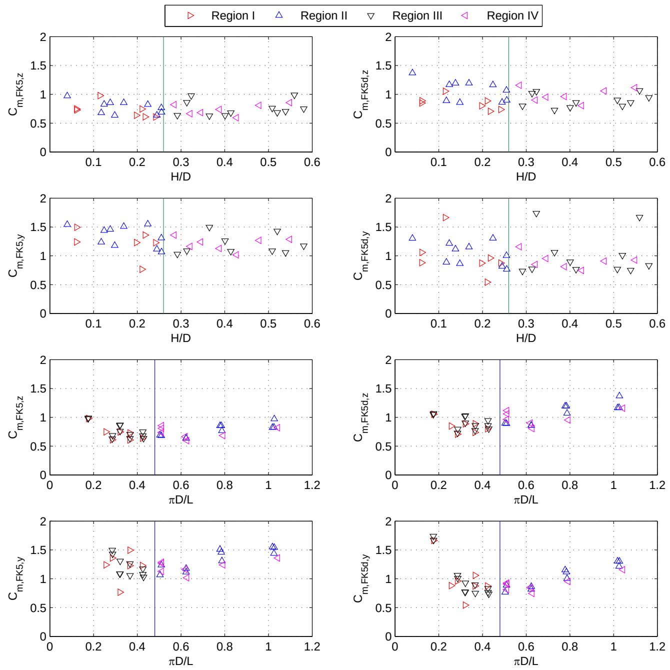

Fig. 20. Vertical and horizontal $C_{m,\text{FK5}}$ (left) and $C_{m,\text{FK5d}}$ (right) against $\frac{H}{L}$ and $\frac{\pi D}{L}$.

For both the vertical and horizontal direction the tests from region II and IV are showing an increase in C_m with higher $\frac{D}{L}$ and no dependency on $\frac{H}{D}$ is observed. Though the difference between the location of $C_{m,\text{FK5}}$ and $C_{m,\text{FK5d}}$ should be noted. In general the improved peak force coefficient is shifted closer to 1 implying that the combined use of Stokes 5$^{\text{th}}$ order theory with the diffraction coefficient, β, makes good estimations on the real wave excitation forces for the entire range of both $\frac{H}{D}$ and $\frac{D}{L}$. The Keulegan-Carpenter number is very low for all 36 tests indicating that no significant drag effects are at work and from the use of the diffraction coefficient the diffraction effects are regarded. Making the rough assumption that the diffraction improved peak force coefficient $C_{m,\text{FK5d}}$ is independent of other parameters it makes sense to calculate the root mean square error (error being $C_m - 1$), the mean value and standard deviation. The results are listed in Table V for all estimation methods and their respective C_m for both vertical and horizontal direction.

TABLE V
PERFORMANCE OF METHODS

	Peak force coefficient	RMS	Mean	Std. dev.
z	$C_{m,\text{WA}}$	0.17	0.96	0.16
	$C_{m,\text{FK1}}$	0.24	0.79	0.12
	$C_{m,\text{FK5}}$	0.27	0.75	0.11
	$C_{m,\text{FK5d}}$	0.16	0.95	0.16
y	$C_{m,\text{WA}}$	0.42	1.14	0.40
	$C_{m,\text{FK1}}$	0.63	1.45	0.44
	$C_{m,\text{FK5}}$	0.50	1.34	0.36
	$C_{m,\text{FK5d}}$	0.27	0.99	0.27

In Table V it is noted that WAMIT is relatively good at estimating the vertical wave excitation forces compared to Stokes 1$^{\text{st}}$ order and 5$^{\text{th}}$ order theory. Only the improved 5$^{\text{th}}$ order Froude-Krylov force is equally good. From the standard deviation the 1$^{\text{st}}$ and 5$^{\text{th}}$ order Froude-Krylov force are relatively stable, though the mean value of $C_{m,\text{FK1},z}$ and $C_{m,\text{FK5},z}$ is rather small.

In the estimation of the horizontal wave excitation forces WAMIT and the 1$^{\text{st}}$ and 5$^{\text{th}}$ order Froude-Krylov force are under predicting the peak forces, indicating that diffraction effects are influencing the results. Only the improved 5$^{\text{th}}$ order Froude-Krylov force gives a good estimation of the measured forces with a very good mean value and a relatively small standard deviation.

The larger standard deviation for the wave excitation forces in the horizontal direction is in general an indication of the diffraction effects influencing the results. The same reason the improved Froude-Krylov force has a lower standard deviation than the other methods.

V. Conclusion

The peak force coefficient C_m defined by Equation 4 is calculated in horizontal and vertical direction for four different estimation methods; linear potential diffraction theory using the commercial tool WAMIT and a calculation of the Froude-Krylov force, F_{FK}, based on either Stokes 1$^{\text{st}}$ order or 5$^{\text{th}}$ order theory. The fourth estimation method utilizes a diffraction coefficient, β, defined in Equation 2 to improve the estimation of the 5$^{\text{th}}$ order Froude-Krylov, by taking both non-linearity and diffraction into account.

Since drag, diffraction and non-linear effects are related to the parameters $\frac{D}{L}$, $K = \frac{U_{\max}T}{D}$ and $s = \frac{H}{L}$ respectively, it is expected to see some changes in C_m when varying the wave height, H, and wave period, T. In the results relatively large variations (e.g. $0.5 \leq C_{m,\text{FK5},y} \leq 1.7$) are seen on C_m within each estimation method, both for horizontal and vertical direction. The only significant trend found was the horizontal and vertical forces depending on $\frac{D}{L}$. This behavior is coincident with the diffraction region for horizontal forces on vertical cylinders [5].

The test data are only located in the inertia and diffraction regions, which explains why no trend towards K is observed. Comparison of the peak force coefficients stability within these regions showed large differences in force prediction precision for the four different estimation methods.

Force prediction using Stokes 1$^{\text{st}}$ order theory was generally the worst estimation method for both directions. This was expected since neither non-linearity nor diffraction is included. The 5$^{\text{th}}$ order Froude-Krylov performed slightly better in the horizontal load prediction due to a better description of non-linearity.

The force prediction using WAMIT yields good results in the vertical direction, but lacks precision in the horizontal direction, due to neglecting surface elevation. The improved Froude-Krylov force prediction model, F_{FK5d}, matches WAMIT in vertical prediction, but radically improves precision when considering horizontal force excitation. The force peak coefficient C_m drops from a mean value of 1.14 with a standard deviation of 0.40 to a mean value of 0.99 with a standard deviation of 0.27.

ACKNOWLEDGMENT

The authors wish to thank the Wavestar company for a helpful collaboration and the members of INORE who participated in giving constructive feedback.

REFERENCES

[1] M. M. Jakobsen, M. M. Kramer, S. Beatty, F. Ferri, and A. Zurkinden, "Experimental study of wave excitation forces on a point absorber," *EWTEC*, 2013.
[2] Wavestar, "Unlimited clean energy," http://wavestarenergy.com, 2013.
[3] WAMIT, "Wamit user manual versions 6.4, 6.4pc, 6.3s, 6.3s-pc," WAMIT Inc. and Massachusetts Institute of Technology, Tech. Rep., 2006.
[4] J. Falnes, *Ocean waves and oscillating systems*. Cambridge: Cambridge University Press, 2002.
[5] T. Sarpkaya, *Wave forces on offshore structures*. Cambridge: Cambridge University Press, 2010.
[6] H. F. Burcharth, *Strøm- og bølgekræfter påstive legemer*, AUC, Sohngaardsholmsvej 57, 9000 Aalborg, Denmark, 2002, vol. 2.
[7] Thomas Lykke Andersen and Peter Frigaard, *Lecture Notes for the Course in Water Wave Mechanics*, AAU, Sohngaardsholmsvej 57, 9000 Aalborg, Denmark, 2011.
[8] S. K. Chakrabarti, *Hydrodynamics of Offshore Structures*. Southamptom: WIT Press, 1987.

Part II

Appendices

A List of digital appendices

A.1 Wave anlysis of experiment

See attached *.m*-file:

`\Regular waves\WaveDetailAtFloat.m`

A.2 Comparison of experiment with calculations

See attached *.m*-files:

`\Regular waves\ExpForceCompare.m`

`\Regular waves\CMtrend.m`

`\Regular waves\ParameterStudy.m`

A.3 Undisturbed, regular force calculation (6 dof)

See attached *.m*-file:

`\Forces\ExpForceCompare.m`

A.4 Undisturbed, regular pressure calculation

See attached *.m*-file:

`\Forces\ExpURpressure.m`

A.5 Undisturbed, Stokes 1. order programs

See attached *.m*-files:

`\Forces\stoke1\pressure1.m`

`\Forces\stoke1\pressure1wheeler.m`

`\Forces\stoke1\wavelength1.m`

A.6 Undisturbed, Stokes 5. order programs

See attached *.m*-files:

`\Forces\stoke5\pressure5.m`

`\Forces\stoke5\stokes5ABC.m`

`\Forces\stoke5\stokes5DE.m`

`\Forces\stoke5\wavelength5.m`

A.7 WAMIT calculation on float

See attached *.m*-files:

`\WAMIT\Wamit_force_output.m`

`\WAMIT\Wamit_Hres_Amp_Phase.m`

`\WAMIT\Wamit_X_read_float.m`

A.8 WAMIT calculation on cylinder

See attached *.m*-file:

`\Pressure integration cylinder\Wamit_X_read.m`

B Experimental setup

Several tests were carried out in the lab with regular waves and a fixed floater. At the time of the experiment the bottom of the tank was removed yielding deeper water depths. This change in depth has changed the incoming waves due to shoaling and refraction and it is therefore needed to find the correct waves at the same point as the floater. For this reason all following wave data is taken from wave gauges at the same distance from the wave generator as the float. On figure B.3 the setup can be seen; float placed at *F2* and wave gauge measurements used are from *WG13*.

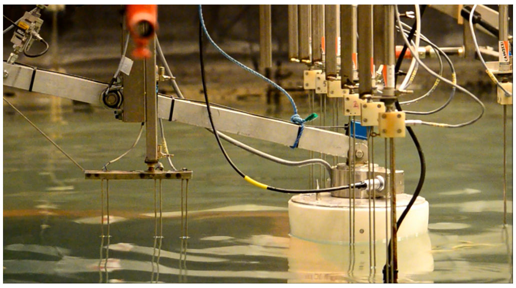

Figure B.1: Experimental setup, wave propagation from left to right.

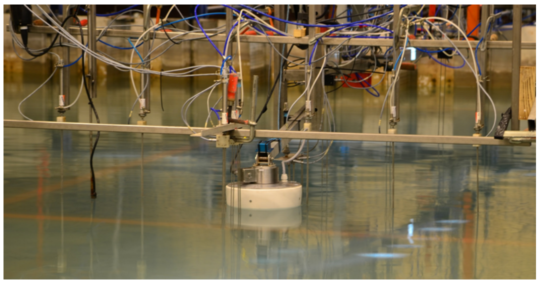

Figure B.2: Experimental setup, wave propagation from background to forground.

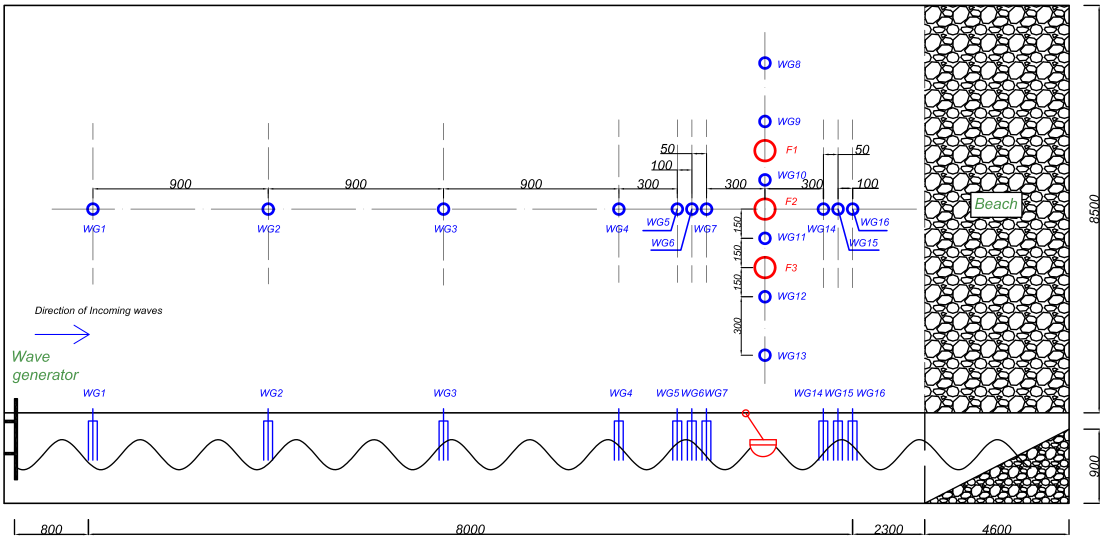

Figure B.3: Experimental setup overview.

B.1 Wave analysis

Due to reflection in the wave tank and the noise from the still water in the begining of the tests it is important to only look at a small part of the test data. This data is then filtered by taking the mean of the four nearest data points in time. In order to find the correct wave height, a zero-down-crossing analysis is carried out on the filtered data, yielding the data shown in figures B.4-B.49.

The data is used to compare with the theoretical calculations of the surface elevation using Stokes 1st order and 5th order theory.

An overview of the wave height, wave period, steepness and surface elevation normalized to the wave height is given in tabel B.1, where both η from the experiment and Stokes 1st order and 5th order theory is given.

				$\eta_{\max}/H$		
Test no.	H	T	s	Experiment	1. order	5. order
[#]	[m]	[s]	[-]	[-]	[-]	[m]
1	0.010	0.700	0.01	0.58	0.50	0.51
2	**0.031**	**0.700**	**0.04**	**0.53**	**0.50**	**0.53**
3	0.056	0.703	0.07	0.63	0.50	0.56
4	0.071	0.694	0.09	0.61	0.50	0.57
5	0.029	0.998	0.02	0.44	0.50	0.52
6	0.064	1.004	0.04	0.54	0.50	0.53
7	0.097	0.996	0.06	0.50	0.50	0.55
8	0.120	0.995	0.08	0.48	0.50	0.56
9	**0.137**	**0.996**	**0.09**	**0.57**	**0.50**	**0.57**
10	0.013	1.074	0.01	0.53	0.50	0.51
11	0.054	1.399	0.02	0.54	0.50	0.52
12	0.091	1.396	0.03	0.56	0.50	0.54
13	0.130	1.392	0.05	0.48	0.50	0.56
14	0.161	1.410	0.06	0.57	0.50	0.57
15	0.182	1.413	0.06	0.64	0.50	0.58
16	**0.029**	**1.987**	**0.01**	**0.53**	**0.50**	**0.52**
17	**0.081**	**1.993**	**0.02**	**0.58**	**0.50**	**0.55**
18	**0.140**	**1.984**	**0.03**	**0.63**	**0.50**	**0.58**
19	0.203	1.993	0.05	0.70	0.50	0.62
20	0.236	1.974	0.05	0.67	0.50	0.63
21	0.013	0.798	0.01	0.40	0.50	0.51
22	0.035	0.801	0.03	0.55	0.50	0.53
23	0.042	0.804	0.04	0.55	0.50	0.53
24	0.064	0.799	0.06	0.52	0.50	0.55
25	**0.086**	**0.797**	**0.09**	**0.59**	**0.50**	**0.57**
26	**0.015**	**1.199**	**0.01**	**0.48**	**0.50**	**0.51**
27	0.060	1.200	0.03	0.51	0.50	0.53
28	0.100	1.198	0.05	0.54	0.50	0.54
29	**0.135**	**1.196**	**0.06**	**0.49**	**0.50**	**0.56**
30	0.162	1.194	0.08	0.55	0.50	0.57
31	0.011	0.898	0.01	0.58	0.50	0.51
32	0.037	0.899	0.03	0.54	0.50	0.52
33	0.061	0.900	0.05	0.55	0.50	0.54
34	0.080	0.902	0.06	0.50	0.50	0.55
35	0.107	0.896	0.09	0.57	0.50	0.57
36	0.014	1.097	0.01	0.52	0.50	0.51
37	0.050	1.105	0.03	0.55	0.50	0.52
38	0.073	1.096	0.04	0.55	0.50	0.53
39	0.104	1.100	0.06	0.52	0.50	0.55
40	0.145	1.100	0.08	0.62	0.50	0.57
41	0.017	1.303	0.01	0.56	0.50	0.51
42	0.053	1.298	0.02	0.52	0.50	0.52
43	**0.078**	**1.300**	**0.03**	**0.51**	**0.50**	**0.53**
44	0.127	1.296	0.05	0.56	0.50	0.56
45	0.162	1.295	0.07	0.56	0.50	0.57
46	0.015	1.501	0.01	0.59	0.50	0.51

Table B.1: Wave data overview.

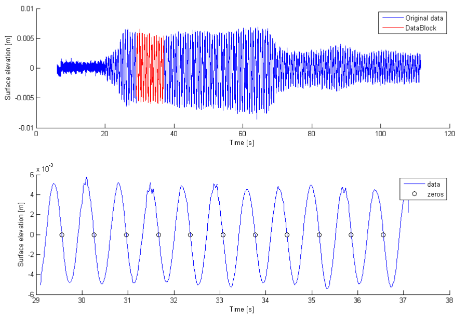

Figure B.4: Wavegauge meassurements at float, test no. 1, $H = 0.0100$ m, $T = 0.6997$ s.

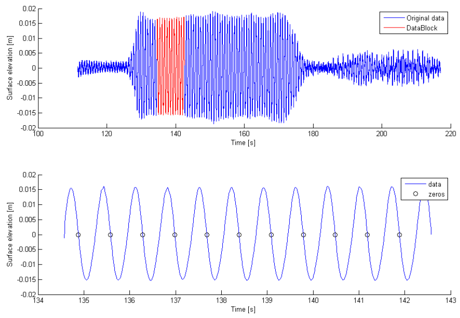

Figure B.5: Wavegauge meassurements at float, test no. 2, $H = 0.0310$ m, $T = 0.7003$ s.

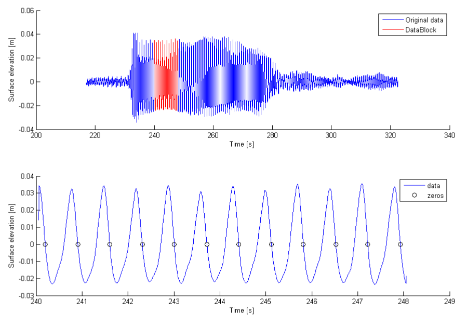

Figure B.6: Wavegauge meassurements at float, test no. 3, $H = 0.0560$ m, $T = 0.7026$ s.

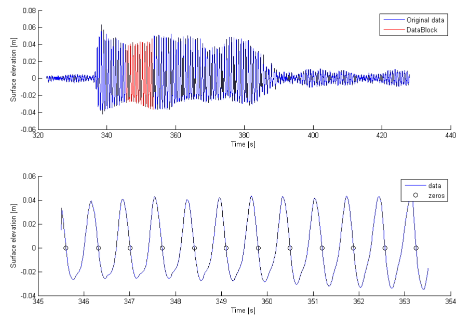

Figure B.7: Wavegauge meassurements at float, test no. 4, $H = 0.0711$ m, $T = 0.6944$ s.

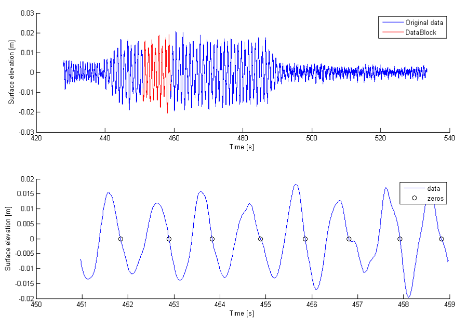

Figure B.8: Wavegauge meassurements at float, test no. 5, $H = 0.0294$ m, $T = 0.9976$ s.

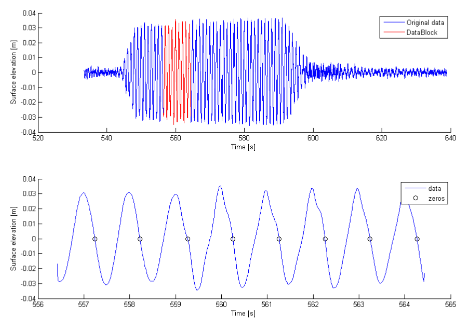

Figure B.9: Wavegauge meassurements at float, test no. 6, $H = 0.0639$ m, $T = 1.0042$ s.

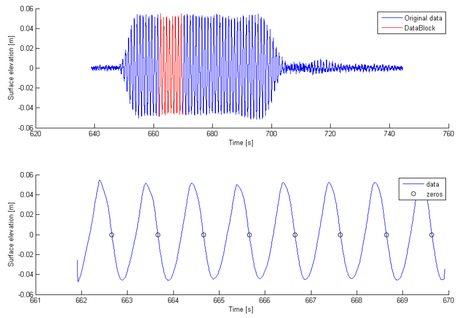

Figure B.10: Wavegauge meassurements at float, test no. 7, $H = 0.0969$ m, $T = 0.9963$ s.

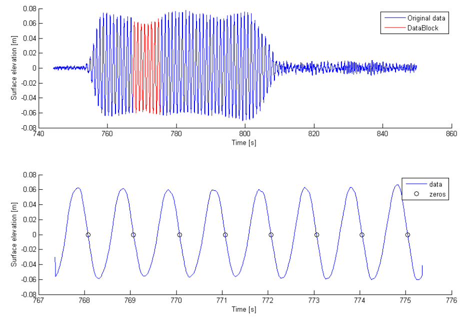

Figure B.11: Wavegauge meassurements at float, test no. 8, $H = 0.1197$ m, $T = 0.9953$ s.

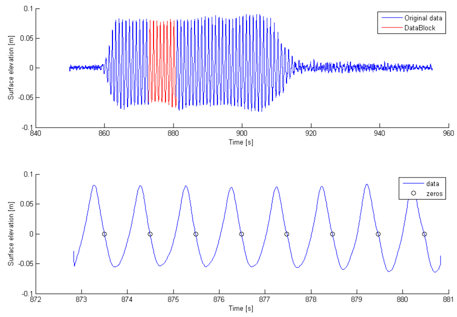

Figure B.12: Wavegauge meassurements at float, test no. 9, $H = 0.1372$ m, $T = 0.9956$ s.

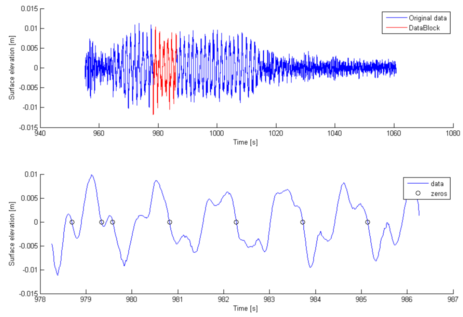

Figure B.13: Wavegauge meassurements at float, test no. 10, $H = 0.0128$ m, $T = 1.0743$ s.

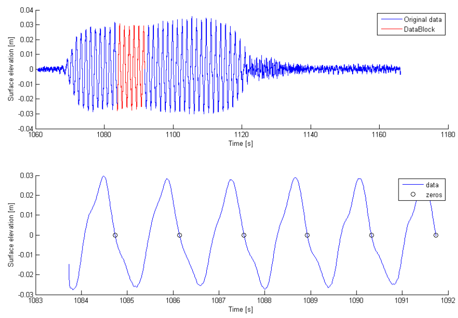

Figure B.14: Wavegauge meassurements at float, test no. 11, $H = 0.0544$ m, $T = 1.3987$ s.

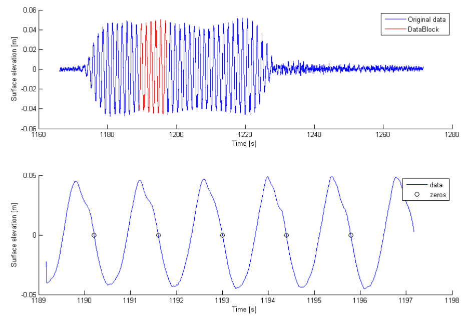

Figure B.15: Wavegauge meassurements at float, test no. 12, $H = 0.0912$ m, $T = 1.3959$ s.

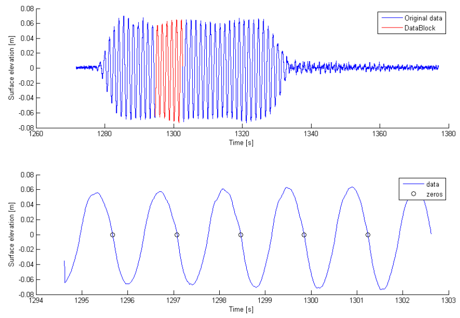

Figure B.16: Wavegauge meassurements at float, test no. 13, $H = 0.1300$ m, $T = 1.3921$ s.

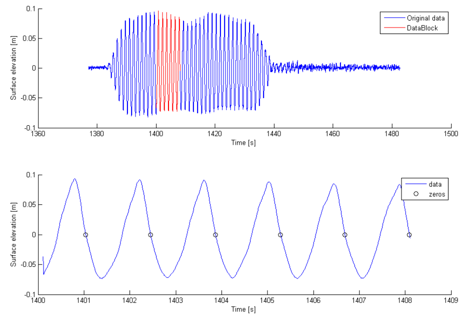

Figure B.17: Wavegauge meassurements at float, test no. 14, $H = 0.1605$ m, $T = 1.4104$ s.

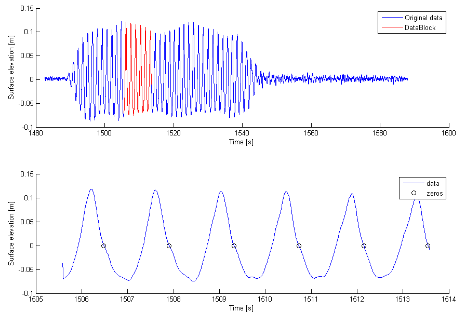

Figure B.18: Wavegauge meassurements at float, test no. 15, $H = 0.1816$ m, $T = 1.4128$ s.

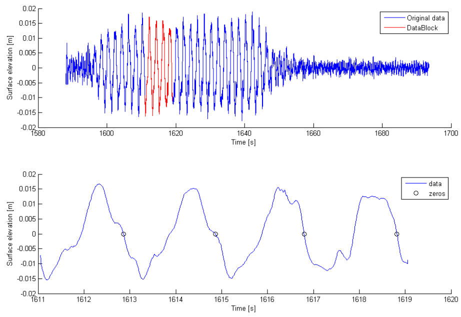

Figure B.19: Wavegauge meassurements at float, test no. 16, $H = 0.0286$ m, $T = 1.9865$ s.

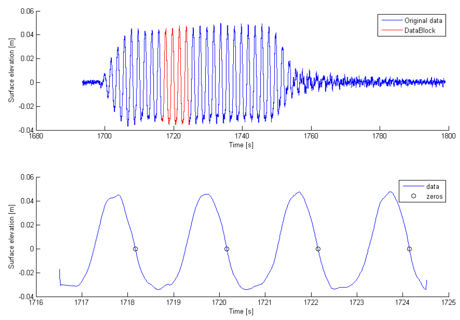

Figure B.20: Wavegauge meassurements at float, test no. 17, $H = 0.0808$ m, $T = 1.9927$ s.

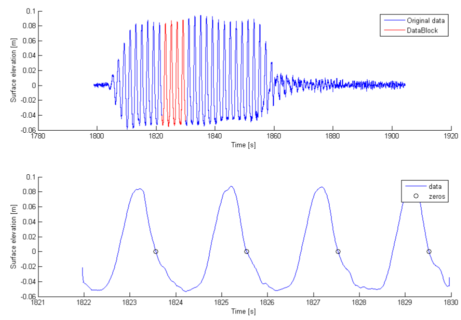

Figure B.21: Wavegauge meassurements at float, test no. 18, $H = 0.1398$ m, $T = 1.9844$ s.

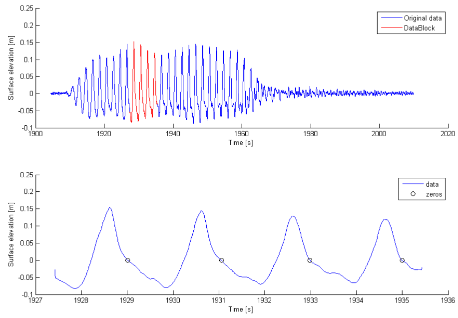

Figure B.22: Wavegauge meassurements at float, test no. 19, $H = 0.2032$ m, $T = 1.9930$ s.

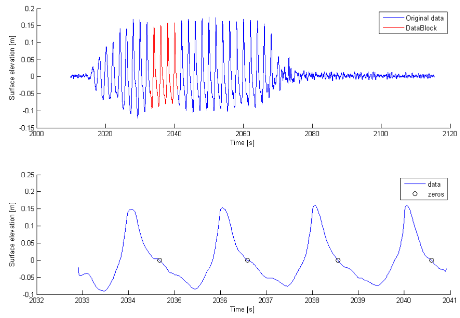

Figure B.23: Wavegauge meassurements at float, test no. 20, $H = 0.2363$ m, $T = 1.9739$ s.

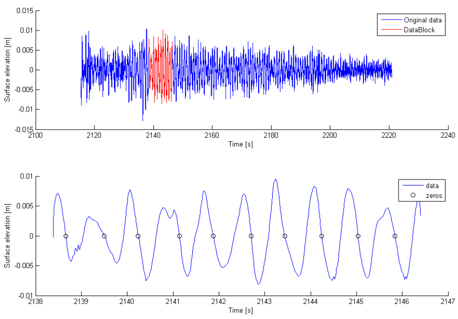

Figure B.24: Wavegauge meassurements at float, test no. 21, $H = 0.0132$ m, $T = 0.7978$ s.

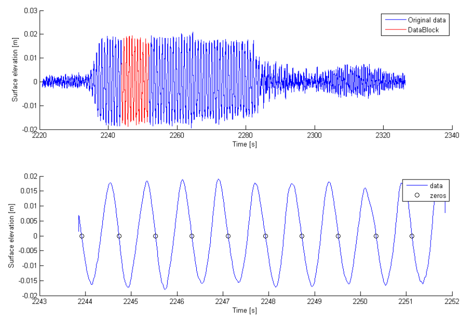

Figure B.25: Wavegauge meassurements at float, test no. 22, $H = 0.0345$ m, $T = 0.8008$ s.

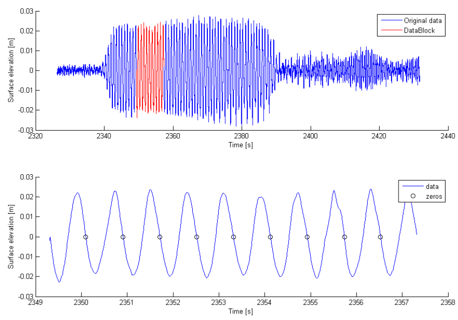

Figure B.26: Wavegauge meassurements at float, test no. 23, $H = 0.0423$ m, $T = 0.8038$ s.

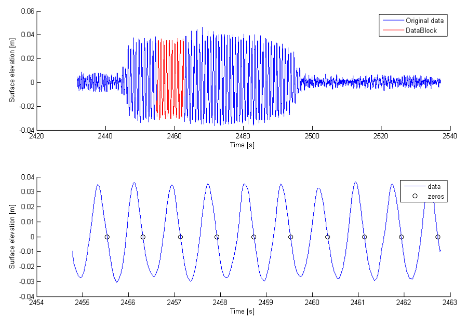

Figure B.27: Wavegauge meassurements at float, test no. 24, $H = 0.0637$ m, $T = 0.7994$ s.

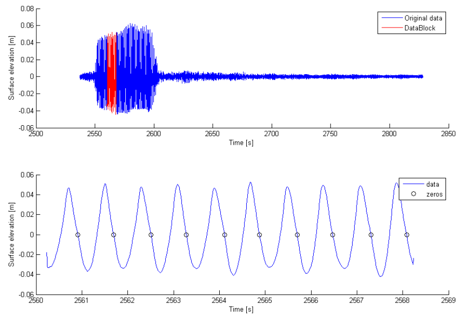

Figure B.28: Wavegauge meassurements at float, test no. 25, $H = 0.0864$ m, $T = 0.7967$ s.

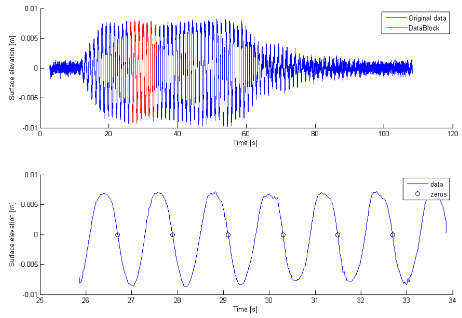

Figure B.29: Wavegauge meassurements at float, test no. 26, $H = 0.0153$ m, $T = 1.1985$ s.

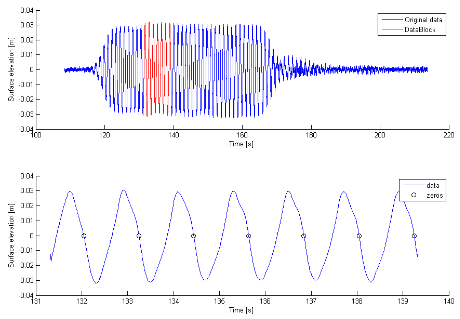

Figure B.30: Wavegauge meassurements at float, test no. 27, $H = 0.0604$ m, $T = 1.1997$ s.

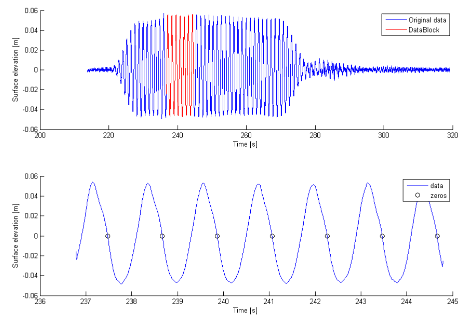

Figure B.31: Wavegauge meassurements at float, test no. 28, $H = 0.1001$ m, $T = 1.1976$ s.

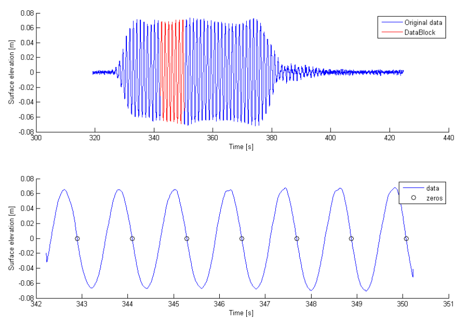

Figure B.32: Wavegauge meassurements at float, test no. 29, $H = 0.1348$ m, $T = 1.1959$ s.

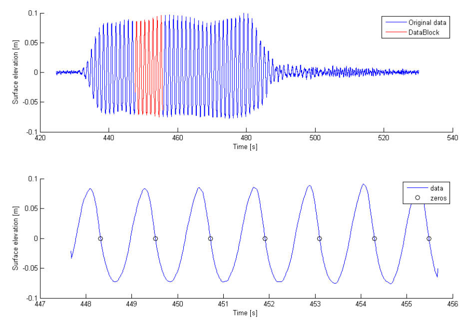

Figure B.33: Wavegauge meassurements at float, test no. 30, $H = 0.1615$ m, $T = 1.1938$ s.

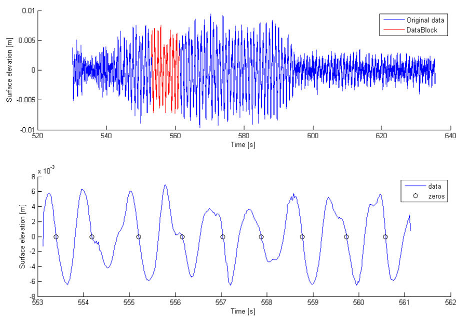

Figure B.34: Wavegauge meassurements at float, test no. 31, $H = 0.0110$ m, $T = 0.8975$ s.

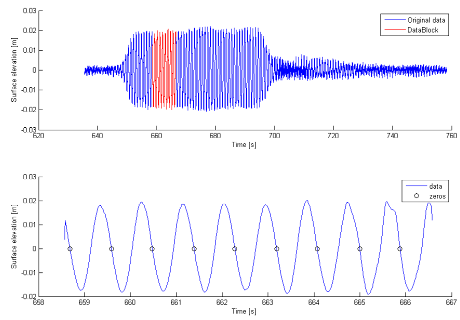

Figure B.35: Wavegauge meassurements at float, test no. 32, $H = 0.0371$ m, $T = 0.8993$ s.

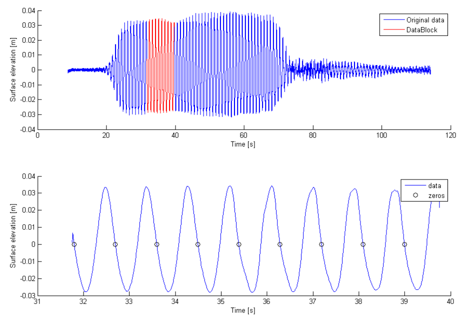

Figure B.36: Wavegauge meassurements at float, test no. 33, $H = 0.0612$ m, $T = 0.8996$ s.

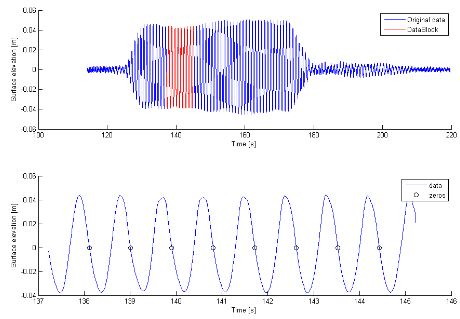

Figure B.37: Wavegauge meassurements at float, test no. 34, $H = 0.0802$ m, $T = 0.9022$ s.

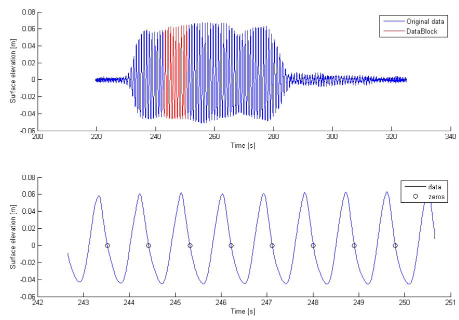

Figure B.38: Wavegauge meassurements at float, test no. 35, $H = 0.1067$ m, $T = 0.8964$ s.

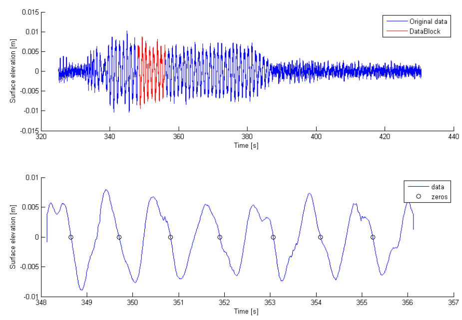

Figure B.39: Wavegauge meassurements at float, test no. 36, $H = 0.0138$ m, $T = 1.0973$ s.

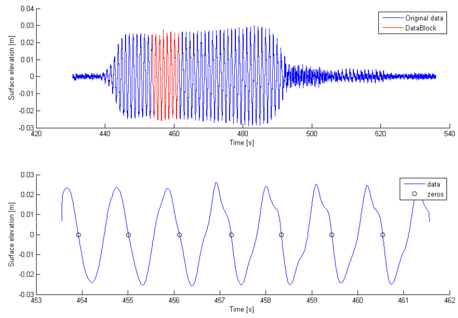

Figure B.40: Wavegauge meassurements at float, test no. 37, $H = 0.0495$ m, $T = 1.1045$ s.

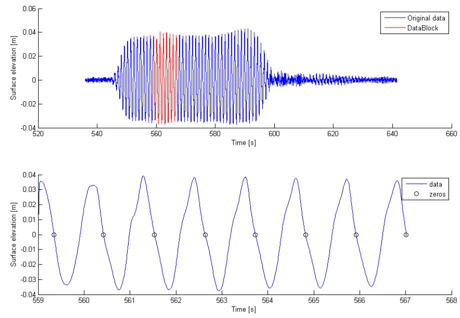

Figure B.41: Wavegauge meassurements at float, test no. 38, $H = 0.0729$ m, $T = 1.0955$ s.

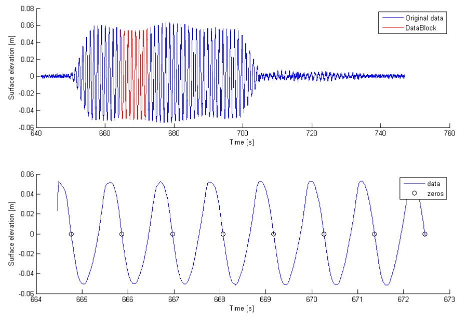

Figure B.42: Wavegauge meassurements at float, test no. 39, $H = 0.1035$ m, $T = 1.0999$ s.

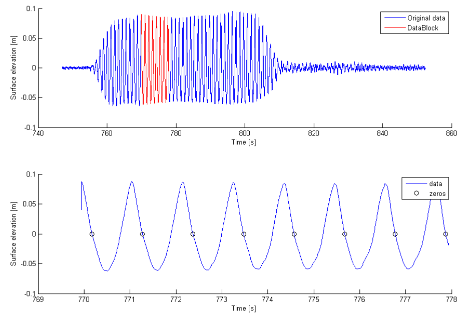

Figure B.43: Wavegauge meassurements at float, test no. 40, $H = 0.1451$ m, $T = 1.0999$ s.

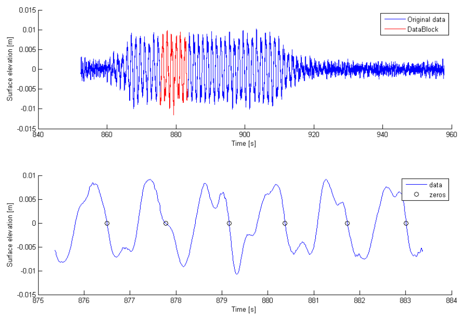

Figure B.44: Wavegauge meassurements at float, test no. 41, $H = 0.0167$ m, $T = 1.3034$ s.

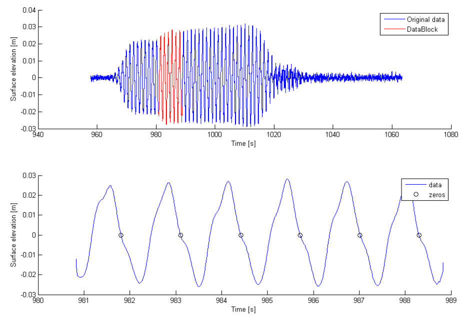

Figure B.45: Wavegauge meassurements at float, test no. 42, $H = 0.0526$ m, $T = 1.2980$ s.

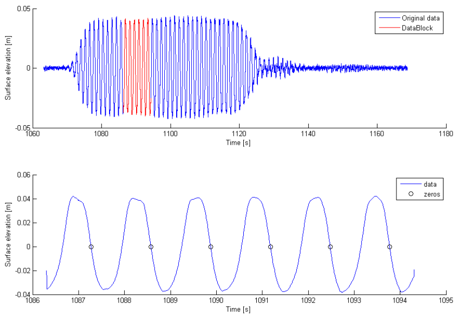

Figure B.46: Wavegauge meassurements at float, test no. 43, $H = 0.0783$ m, $T = 1.2998$ s.

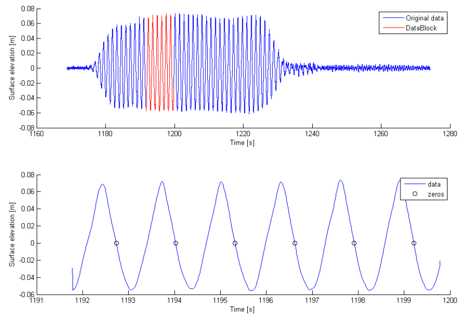

Figure B.47: Wavegauge meassurements at float, test no. 44, $H = 0.1271$ m, $T = 1.2956$ s.

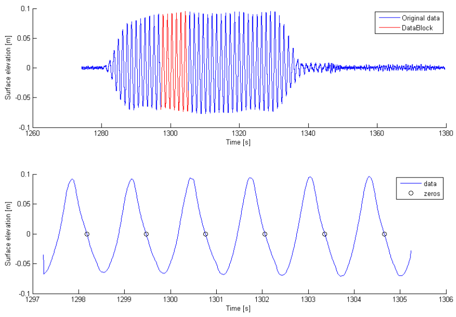

Figure B.48: Wavegauge meassurements at float, test no. 45, $H = 0.1618$ m, $T = 1.2949$ s.

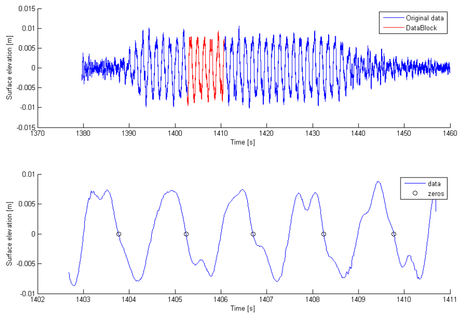

Figure B.49: Wavegauge meassurements at float, test no. 46, $H = 0.0152$ m, $T = 1.5013$ s.

C Wave theories used for the investigation

The analysis of the point absorber focus on the difference in disturbed and undisturbed wave fields around the point absorber in order to estimate a design factor to be used with faster undisturbed calculations for a preliminary calculation of the pressures and forces on the point absorber. These pressures and forces is then to be used for the design of the shell.

The program used to calculate the disturbed wave field, WAMIT, is based on Stokes 1st order theory and uses equations for incomming waves and scattered waves together with the superposition principle in order to calculate the disturbed wave field.

The undisturbed forces and pressures are found using different available wave theories, were the focus is on Stokes 1st and 5th order theory and Deans Stream function theory. The forces are found by integrating the presures over the wetted surface of the point absorber and a generel equation of the undisturbed pressure is given by the generelized Bernoulli Equation (C.1).

$$\begin{aligned} p &= p_h + p_d \\ &= -\rho g z - \rho \left[\frac{1}{2}\left(u^2 + w^2\right) + \frac{\partial \phi}{\partial t} \right] \end{aligned} \tag{C.1}$$

p_h	hydrostatic pressure
p_d	dynamic presure
ρ	density of water
g	gravitational acceleration
z	vertical position with respect to mean water level
u	horizontal velocity
w	vertical velocity
ϕ	velocity potential
t	time

The hydrostatic pressure is only depending on the position relative to the mean water level and can be found relatively easy. The dynamic pressure depends on the particle velocity and the velocity potential of the wave field, from which the particle velocities can also be found.

Both Stokes theory and Deans stream function theory is based on solving the Laplace equation of the water flow, assumed that the flow is irrotational and invicid.

C.1 Stokes waves

The theory is based on the velocity potential and the Laplace equation as shown in equation (C.2).

$$\frac{\partial^2 \phi}{\partial x^2} + \frac{\partial^2 \phi}{\partial z^2} = 0 \tag{C.2}$$

The velocity potential is the analytical solution to the Laplace equation and in order to solve the equation certain assumptions are made with regards to the surface boundary condition in the wave field.

For Stokes 1st order theory the wave height is assumed negligibly small compared to the wave length and the water depth. This makes the theory applicable only for a certain range of ocean conditions.

For Stokes 5th order waves (or any given non-linear stokes theory) the pertubation method is used in order to find the non-linear terms. The assumption is again that the higher order terms can be neglected. Here the assumption of the order of the wave height divided by the water depth is equal to 1 makes the theory applicable only for a certain range of ocean conditions (problems occur at shallow water) since the physics breaks down and secondary wave crests starts to form at the wave trough.

All stokes waves have an approximate surface and the theory breaks down in the range of the mean water level. For stokes 1st order theory the profile is stretched to the water surface using wheeler stretching and the pressure found by stokes 5th order theory is forced to zeroat the surface using the Bernoulli Constant.

C.2 Deans Stream function waves

Deans stream function theory is based on an approximate sollution to the Laplace equation solved at the exact surface boundary. In this way there are no assumptions on the order of $\frac{H}{L}$ or $\frac{h}{L}$. This elliminates the probles found using Stokes theory at shallow water, though the theory still breaks down close to the breaking limit and when at really shallow water.

Deans stream function theory assumes that the flow is travelling with the current and for this reason the flow is steady and the velocity potential is zero. Instead the stream function is introduced as the sollution to the Laplace equation as shown in equation (C.3).

$$\frac{\partial^2 \psi}{\partial x^2} + \frac{\partial^2 \psi}{\partial z^2} = 0 \tag{C.3}$$

C.3 Theory application

As discussed, then the different theories have various application areas. Stokes theory gets better and better with more non-linear terms regarded, though also more cumbersome in the calculation. Figure C.1 shows the areas of application.

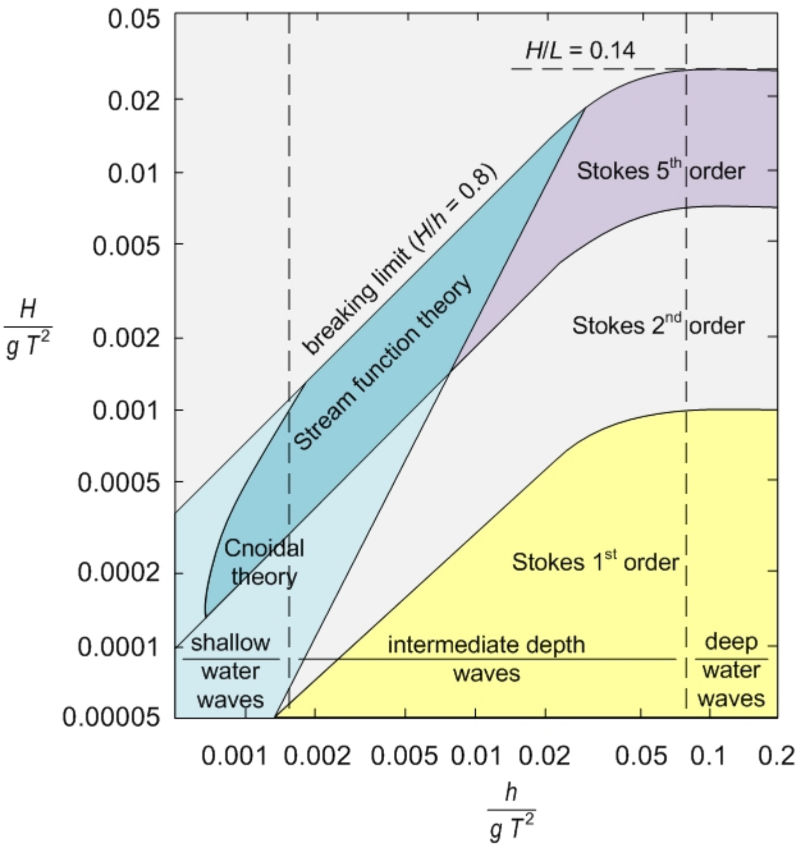

Figure C.1: Application area of different wave theories.

D Undisturbed pressure model

The undisturbed pressure on the float shell can be described by the Froude-Krylov theorem, see (D.1).

$$\vec{F}_{FK} = -\iint_{S_w} p\,\vec{n}\,ds \tag{D.1}$$

$\vec{F}_{FK}$	Froude-Krylov force
S_w	Wetted surface
p	Undisturbed pressure
$\vec{n}$	Normal vector

To be able to utilize this theory along with a calculated pressure field, an element model is needed. From the given geometries of the 1:20 float used in the experimental tests a CAD model is drawn and segmented into a grid of triangular panels.

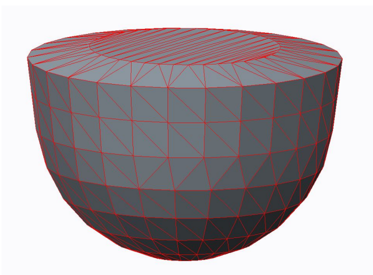

Figure D.1: Segmented CAD model. This model was later discarded due to the ueven propotions of elements on lid.

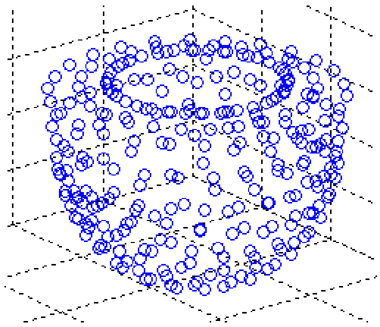

Figure D.2: Scatter of element nodes loaded into MATLAB.

When coordinates of the element nodes are known the geometrical properties of centroid, area and normal can determined, see (D.2), (D.3) and (D.4).

$$\vec{CT}_i = \frac{\vec{A}_i + \vec{B}_i + \vec{C}_i}{3} \tag{D.2}$$

$\vec{CT}_i$	Centroid coordinate vector
$\vec{A}_i$	Coordinate vector of first node
$\vec{B}_i$	Coordinate vector of second node
$\vec{C}_i$	Coordinate vector of third node

$$\begin{aligned} T_i &= \sqrt{s_i(s_i - a_i)(s_i - b_i)(s_i - c_i)} \\ s_i &= \frac{a_i + b_i + c_i}{2} \end{aligned} \tag{D.3}$$

T_i	Area of element
s_i	Semiperimeter of element
a_i	First side length
b_i	Second side length
c_i	Third side length

$$\vec{n}_i = \vec{U}_i \times \vec{V}_i \qquad (D.4)$$
$$\vec{U}_i = \vec{B}_i - \vec{A}_i$$
$$\vec{V}_i = \vec{C}_i - \vec{A}_i$$

$\vec{n}_i$	Normal vector of element
$\vec{U}_i$	First side vector
$\vec{V}_i$	Second side vector

As the geometric properties are established the forces and moments can be found as summations over all panel segments of the entire float shell, see (D.5) and (D.6).

$$\vec{F} = -\sum_{i=1}^{n} p_i \, T_i \, \vec{n}_i \qquad (D.5)$$

$$\vec{M} = -\sum_{i=1}^{n} \vec{r}_i \times (p_i \, T_i \, \vec{n}_i) \qquad (D.6)$$

$\vec{F}$	Force vector
$\vec{M}$	Moment vector
p_i	Pressure at element centroid
$\vec{r}_i$	Arm vector of element

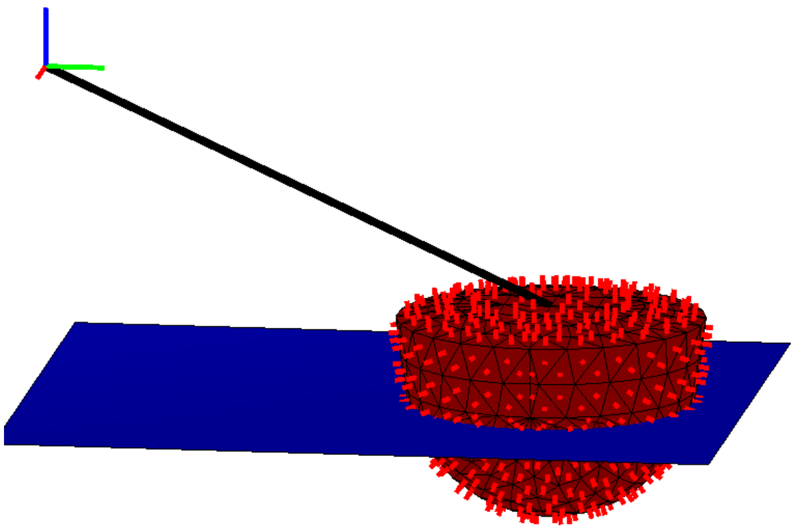

Figure D.3: Final element model. Mean water level and normals are included for illustrative purposes.

E Forces on cylinder

To describe the excitation force from waves on a body submerged in water, the numerical tool WAMIT [2006] is used. As a verification of the results obtained, and a verification of the way these results are read into and analyzed in the pressure integration program, a comparison with an analytical solution is carried out. The model used is a cylinder in comparable scale to the float used in the experiments, i.e. diameter $\text{Ø} = 0.25$ m and water depth $h = 0.65$ m. The model can be seen in figure E.1.

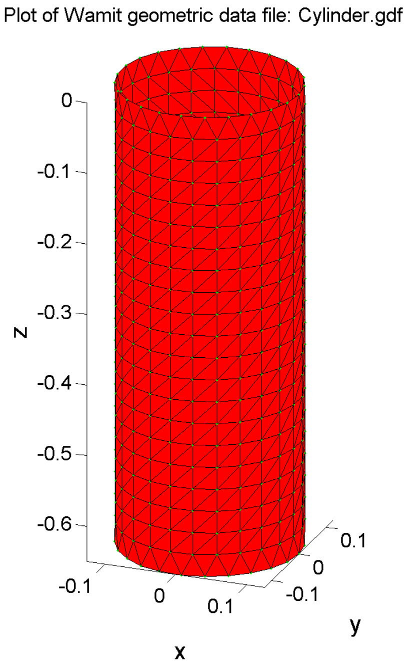

Figure E.1: Element model used for numerical solution.

E.1 MacCamy-Fuchs solution

For a cylinder exposed to first order waves the excitation forces are analytically determined. The analytical solution of the horizontal excitation force can be found in [1]. In figure E.2 and E.3 the force amplitude and phase are shown.

[1] FiXme Note: husk kilde på Sarpkaya

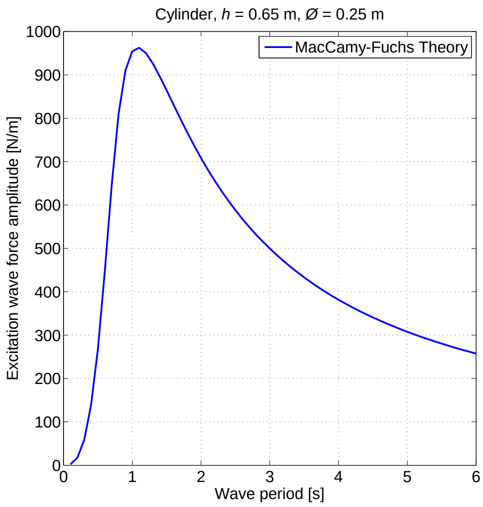

Figure E.2: Analytical first order solution to force amplitude.

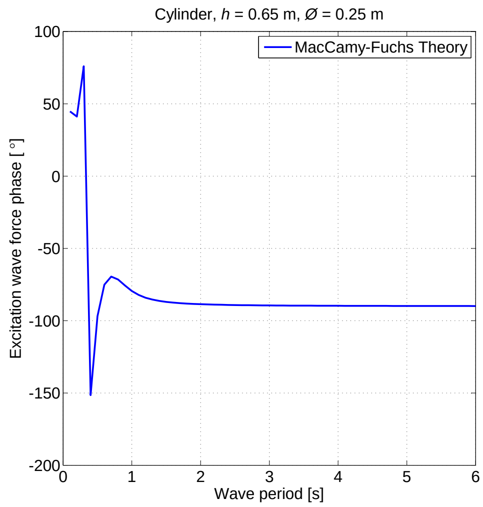

Figure E.3: Analytical first order solution to force phase.

E.2 Numerical solution

When considering excitation force amplitude and phase the WAMIT output reads as seen in figure E.4. Since only the horizontal force is solved analytically, only the one corresponding degree of freedom will be considered in calculation.

$$\text{OPTN.3:} \qquad \text{PER} \quad \text{BETA} \quad \text{I} \qquad \text{Mod}(\bar{X}_i) \quad \text{Pha}(\bar{X}_i) \quad \text{Re}(\bar{X}_i) \quad \text{Im}(\bar{X}_i)$$

Figure E.4: Output format of WAMIT *.3 file [WAMIT, 2006]

Force pr. wave amplitude can from the *.3 output be determined from two expressions, see equation (E.1) and (E.2).

$$f_e(t) = \rho \cdot g \cdot \text{Mod}(\bar{X}_i)\ \cos\left(\omega \cdot t + \text{Pha}(\bar{X}_i)\right) \tag{E.1}$$

or alternatively

$$f_e(t) = \text{Real}\left(H \cdot e^{(\ i \cdot \omega \cdot t)}\right) \tag{E.2}$$
$$H_e(t) = \rho \cdot g \cdot (\text{Re}(\bar{X}_i) + i \cdot \text{Im}(\bar{X}_i)) = \rho \cdot g \cdot \bar{X}_i$$

The force amplitude and phase are plotted along with the analytical solution in figure E.5 and E.6.

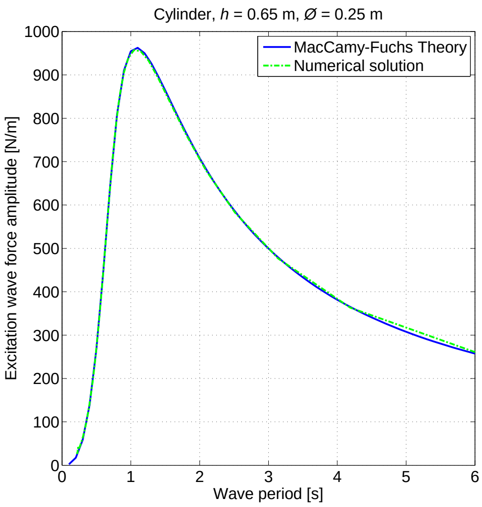

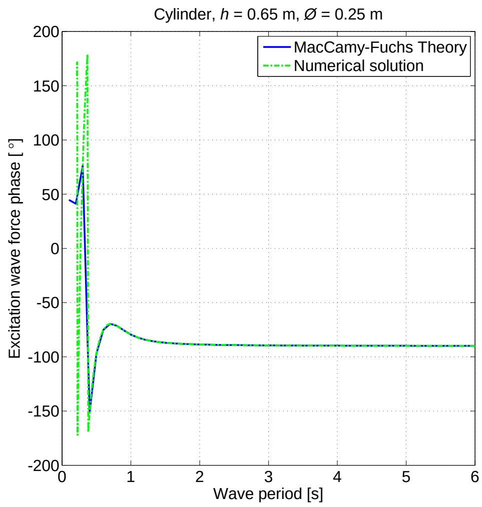

Figure E.5: Numerical first order solution to force amplitude.

Figure E.6: Numerical first order solution to force phase.

E.3 Integrated solution

The pressures found in WAMIT [2006] are summarized over the entire float shell as described in appendix D. The amplitude and phase of peak force over a time interval are calculated for the same periods used for the direct numerical excitation output. In figure E.7 and E.8 it is seen that all three approaches match up very well. The error seen in the phase of lower periods are due to numerical instability as the wave periods becomes relatively small compared to the element size of the numerical model, but even in this area to two different approaches to the numerical solution yields the same results and hereby further verifies the pressure integration approach. As a guideline this numerical instability is expected to occur around wavelengths of 8 times the element size.[2]

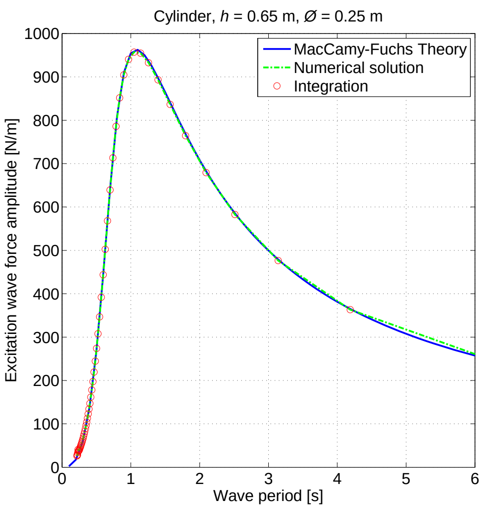

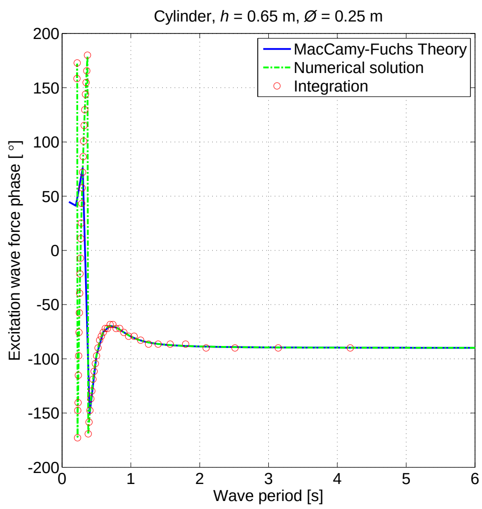

Figure E.7: Force amplitudes of the three different approaches.

Figure E.8: Force phases of the three different approaches.

[2]FiXme Note: Cite her? Kramer tommelfinger-regel

F Numerical forces on float shell

To determine the excitation forces on the float shell different WAMIT models are run. Unlike the model of the cylinder, two degrees of freedom will be considered, i.e. horizontal and vertical force. Since WAMIT is a first order solution, the geometry is cut off at mean water level. This have, in some rare cases, shown to produce standing waves inside the geometry and thus spoiling the solution. To make sure this is not the case, the model is run both with and without a generated *model lid* at mean water level. Further more two models are run to obtain better understanding of the influence of the vertical position of the float. The primary model is places at the level of natural buoyancy of the float and the secondary model is submerged to a level where the top of the model is aligned with the mean water level.[1] The model can be seen in figure F.1, and the water depth is $h = 0.65$ m.

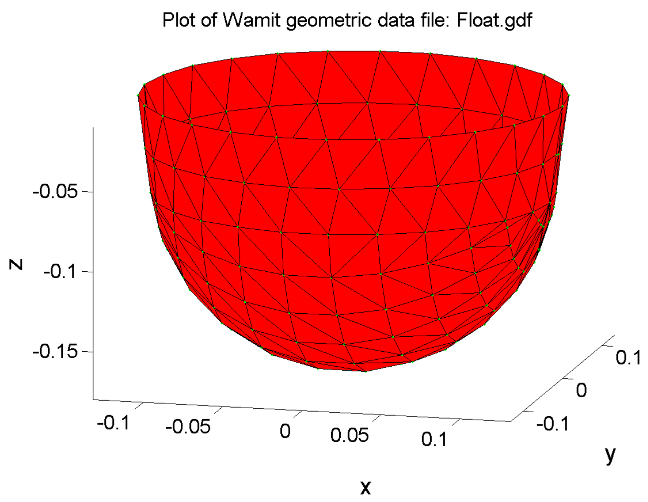

Figure F.1: Element model used for numerical solution.

[1] FiXme Note: ret boyancy til buoyancy i all figs

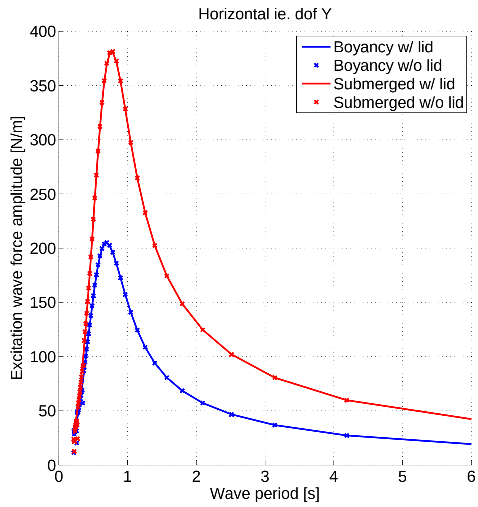

Figure F.2: Horizontal force amplitude.

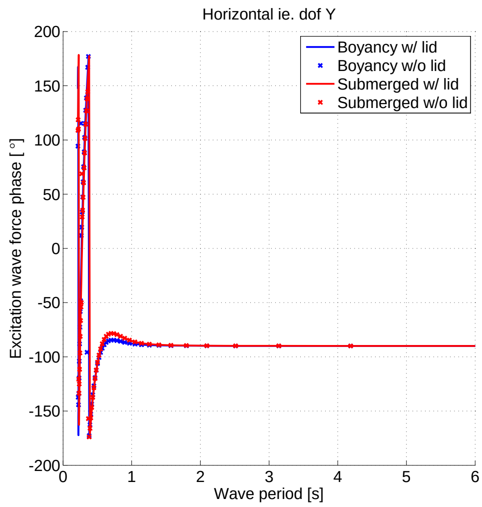

Figure F.3: Horizontal force phase.

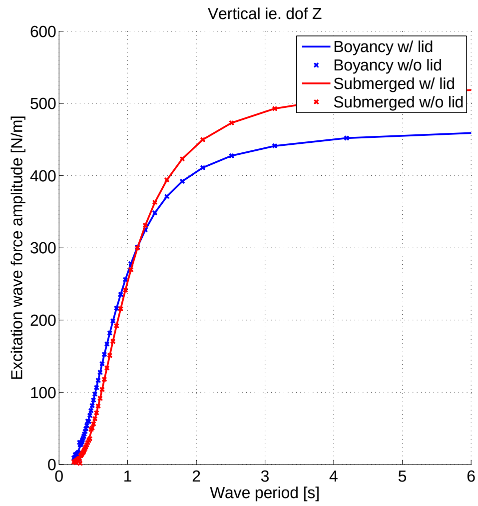

Figure F.4: Vertical force amplitude.

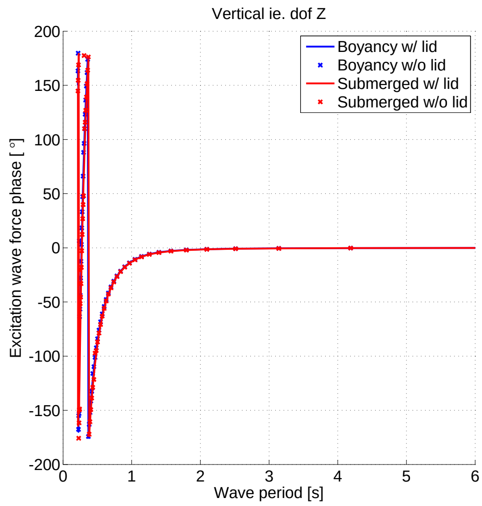

Figure F.5: Vertical force phase.

From figure F.2 and F.3 it is seen that the behavior of the horizontal excitation at higher periods converges to 0 force amplitude at a 90° phase. In the same way figure F.4 and F.5 shows the vertical excitation at higher periods converges to a finite force amplitude at a 0° phase.

G Maximum force vs. wave period approach

In appendix F the Force amplitude dependency of the wave period was plotted using the results from WAMIT. The same approach is used in the following to see if the same dependency when using the undisturbed pressure program described in appendix D. The results are further compared to the test done in the laboratory.

Since Stokes 5th order theory is not linear the superposition principle do not apply. For this reason four different approximate wave heights are investigated from the experiment. It is wanted to have an idea of the whole range of wave heights wave periods, so test from the experiments are with approximate wave heights of $H = 0.03$ m, $H = 0.06$ m, $H = 0.16$ m and $H = 0.24$ m, which have 1 or more different wave periods as well. An overview of the chosen test can be seen in table G.1

H approx [m]	Test no. [#]	H real [m]	T [s]
0.03	2	0.0310	0.7003
0.03	5	0.0294	0.9976
0.03	16	0.0286	1.9865
0.03	22	0.0345	0.8008
0.06	6	0.0639	1.0042
0.06	24	0.0637	0.7994
0.06	27	0.0604	1.1997
0.06	33	0.0612	0.8996
0.16	30	0.1615	1.1938
0.16	45	0.1618	1.2949
0.24	20	0.2363	1.9739

Table G.1: Overview of tests used in approach.

To compare with the undisturbed program the same approximate wave heights are chosen. For each wave a range of wave periods $T = 1 - 3$ s are used to make similar plots to those made in appendix F. The results are shown and commented in the following.

G.1 Maximum Fy and Fz wave excitation forces on floater

First the results using the undisturbed pressure program is compared to the experiment and later the results from WAMIT.

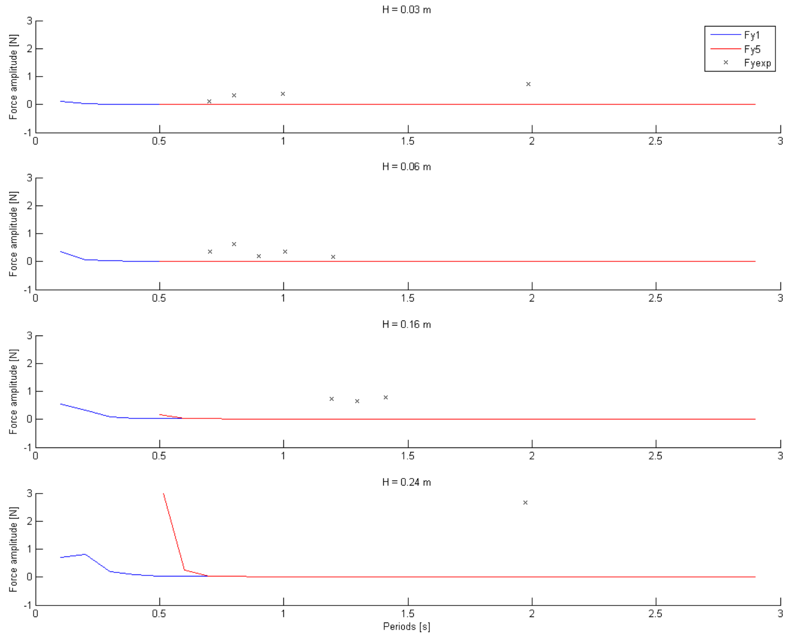

Figure G.1: Horizontal force amplitude comparrison between experiment and undisturbed pressure program.

The horizontal forces from the undisturbed pressure program does not match figure G.1. Since the undisturbed pressure program does not take into account the added mass and the dimension of the floater is very large compared to the wave lengths, then the program does not give the same results.

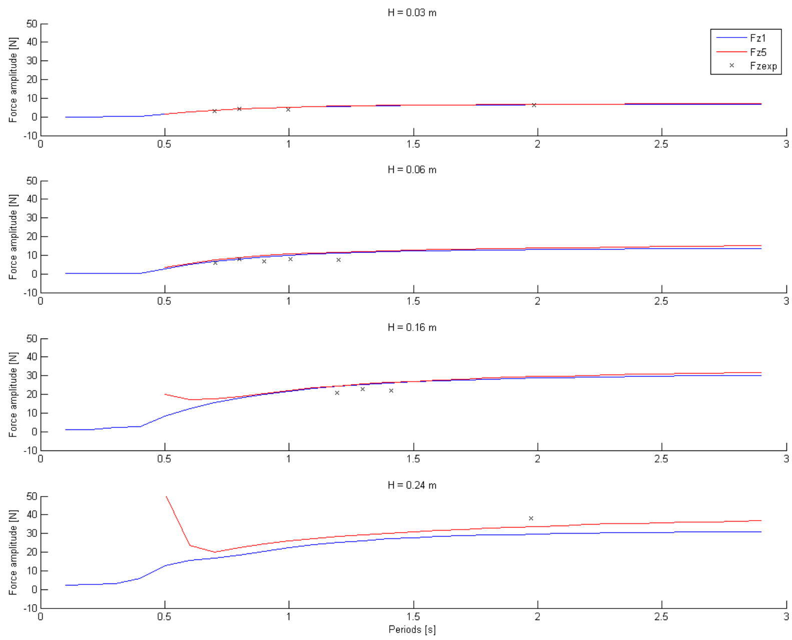

Figure G.2: Vertical force amplitude comparrison between experiment and undisturbed pressure program.

The vertical forces sem to be very well described using the undisturbed pressure program. In order to get the same figures as in appendix F a normalization agains the actual wave height is made, see figure G.3.

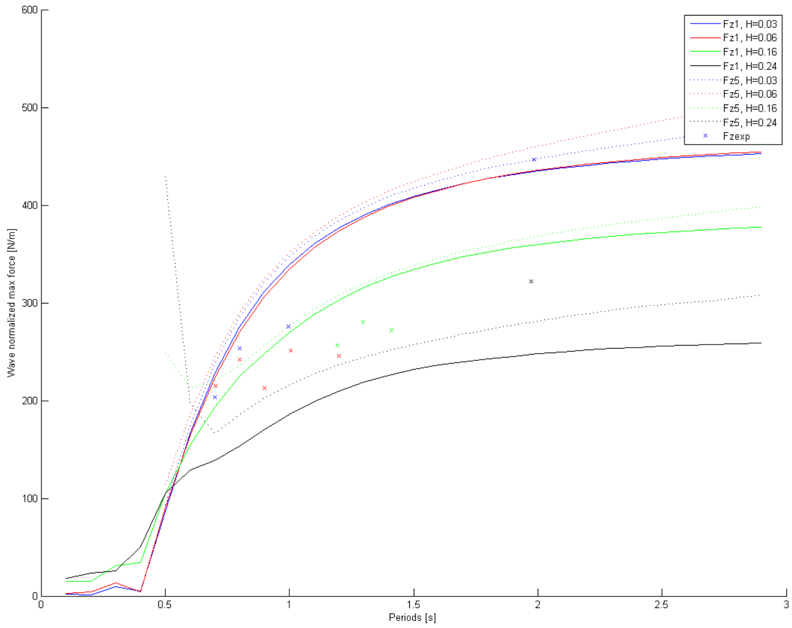

Figure G.3: Normalized maximum **vertical** force from experiment and undisturbed pressure program.

When the normalization is made the fitting is less impressive and it is hard to say if the undisturbed pressure program is usefull. There are no tendencies since the program overestimates at $H = 0.03$ m, $H = 0.06$ m and $H = 0.16$ m and underestimates at $H = 0.24$ m.

It can also be observed that the lines representing Stokes 1st order theory are not close to each other, which was expected.

For a comparrison with WAMIT it is interesting to see how well that program fits to the experiment. The fit to both horizontal and vertical forces can be seen in figure G.4 and G.5.

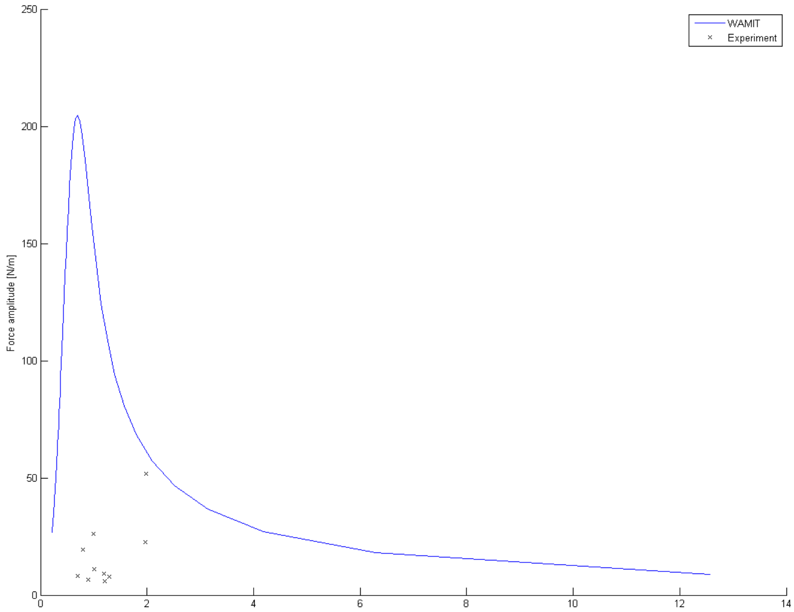

Figure G.4: Force amplitude comparrison between WAMIT and experiment in Fy.

The horizontal forces from WAMIT fits better but there are still some errors.

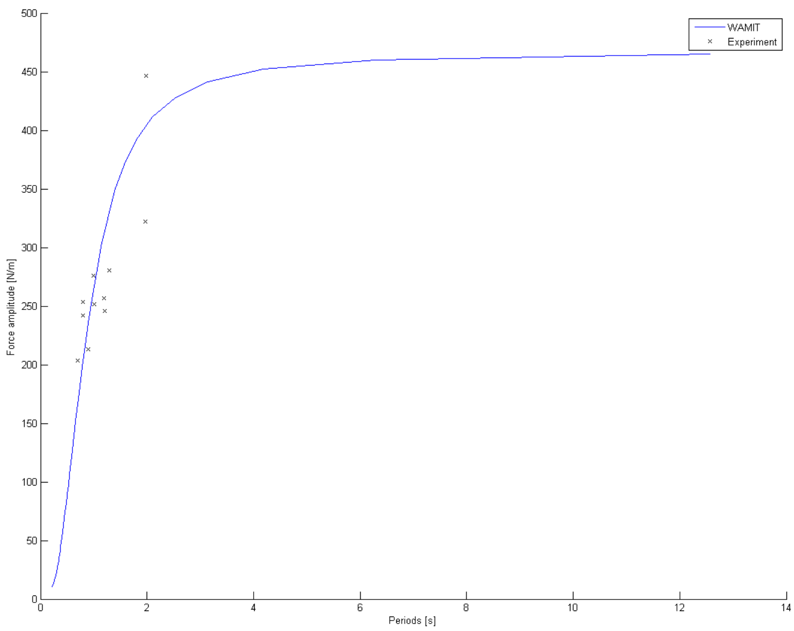

Figure G.5: Force amplitude comparrison between WAMIT and experiment in Fz.

The vertical forces from WAMIT fits very good to the experiments, just like the undisturbed pressure program.

H 3x3 overview approach

A rough comparrison between experiments, WAMIT and the undisturbed pressure program, see appendix D, is wanted.

In order to have an idea of how well the different approaces fit the data from the experiment, a 3 by 3 matrix is made. In this matrix the wave period and the wave height is changed for each index.

From the knowledge of the different wave periods and wave heights at the floater, a proper spred is chosen, so a good estimation of the entire test range can be made, see table H.1.

H \ T	≤ 1.0 s	$1.1 - 1.9$ s	≥ 1.9 s
≤ 0.05 m	2	26	16
$0.06 - 0.10$ m	25	43	17
$0.11 - 0.24$ m	9	29	18

Table H.1: Range of wave periods and wave height and the resulting test numbers.

From the previous zero-down-crossing analysis, the correct wave height and periods for the chosen test data is shown in table H.2 and H.3, given in the same setup as table H.1.

0.031	0.015	0.029
0.086	0.078	0.081
0.137	0.135	0.140

Table H.2: Wave height for the nine chosen tests, given in the unit [m].

0.700	1.199	1.987
0.797	1.300	1.992
0.996	1.196	1.984

Table H.3: Wave periods for the nine chosen tests, given in the unit [s].

An estimate of the steepness of the test data is also found using the dispersion relationship from Stokes 1st order theory. The steepness is listed in table H.4.

0.041	0.007	0.006
0.087	0.032	0.018
0.089	0.063	0.031

Table H.4: Wave steepness for the nine chosen tests, given in the unit $[-]$.

It is important to know which theories are applicable for the different chosen tests. In order to find out the tests are plotted on figure H.1, where the areas of application of the different wave theories can also be seen.

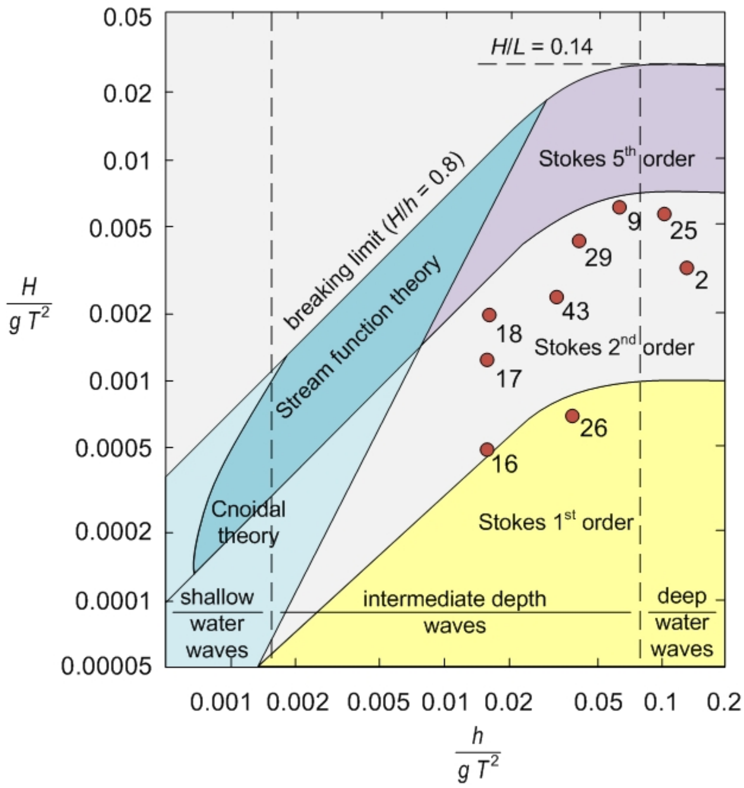

Figure H.1: Overview of test used data and the theoretical applications.

The same test numbers are marked in table B.1 with bold.

H.1 Investigation of selected data

From figure H.1 it is seen that Stokes 1st order theory might not be very good. In order to see wether that is true or not, the surface elevation of the nine different tests are plotted against Stokes 1st order and 5th order theory.

The phase of the theoretical data is shiftet, so it fits the measurements from the wave gauges at the floater.

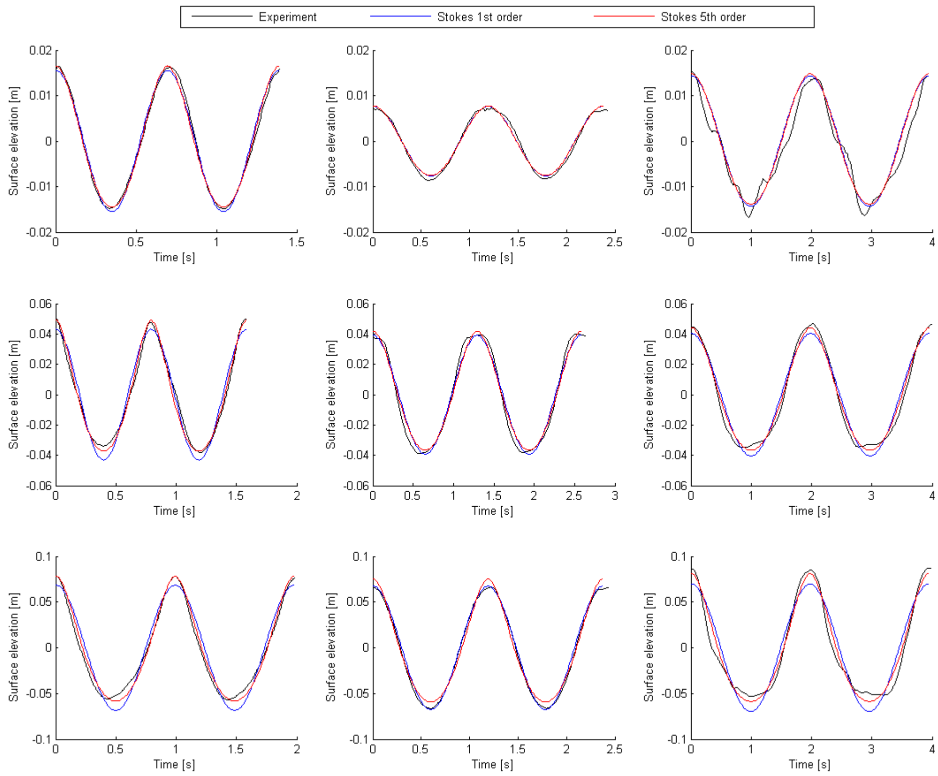

Figure H.2: Comparrison of Surface elevation from chosen tests with theory.

Observations show that in general Stokes 5th order theory fits best to the experiments, which was expected from looking at figure H.1.

I 3x3 force comparrison

In this appendix a force comparrison between the experiment, WAMIT and the undisturbed pressure program, using the same setup as in appendix H, using table H.1, which applicable theory can be found from looking at figure H.2.

So far three different approaches have been made towards finding the forces on the floater: WAMIT, undisturbed program and experiments.

In order to have an idea of the coefficients, the horizontal velocitiesare listed, the Keulegan-Carpenter numer is listed, calculated using equation (I.1).

$$KC = \frac{U_{\max} T}{D} \tag{I.1}$$

KC	Keulegan-Carpenter number
$U_{\max}$	Maximum horizontal force at mean water level
T	Wave period
D	Diameter of float

The velocity is calculated using Stokes 1st order theory.

0.14	0.04	0.06
0.34	0.20	0.18
0.44	0.37	0.31

Table I.1: Maximum horizontal velocities at mean water level, with the unit [m/s].

0.39	0.20	0.50
1.09	1.06	1.41
1.74	1.77	2.43

Table I.2: KC number.

The steepness and maximum surface elevation normalized to the wave height is also shown in order to have an idea of the behaviour.

0.04	0.01	0.01
0.09	0.03	0.02
0.09	0.06	0.03

Table I.3: Wave steepness.

0.53	0.48	0.53
0.59	0.51	0.58
0.57	0.49	0.63

Table I.4: $\frac{\eta_{\text{exp,max}}}{H}$.

From figure H.2 it is seen that Stokes 1st order theory might not be very good. In order to see wether that is true or not, the nine different tests are plotted against WAMIT and the undisturbed wave field program, see figure I.1 and I.2.

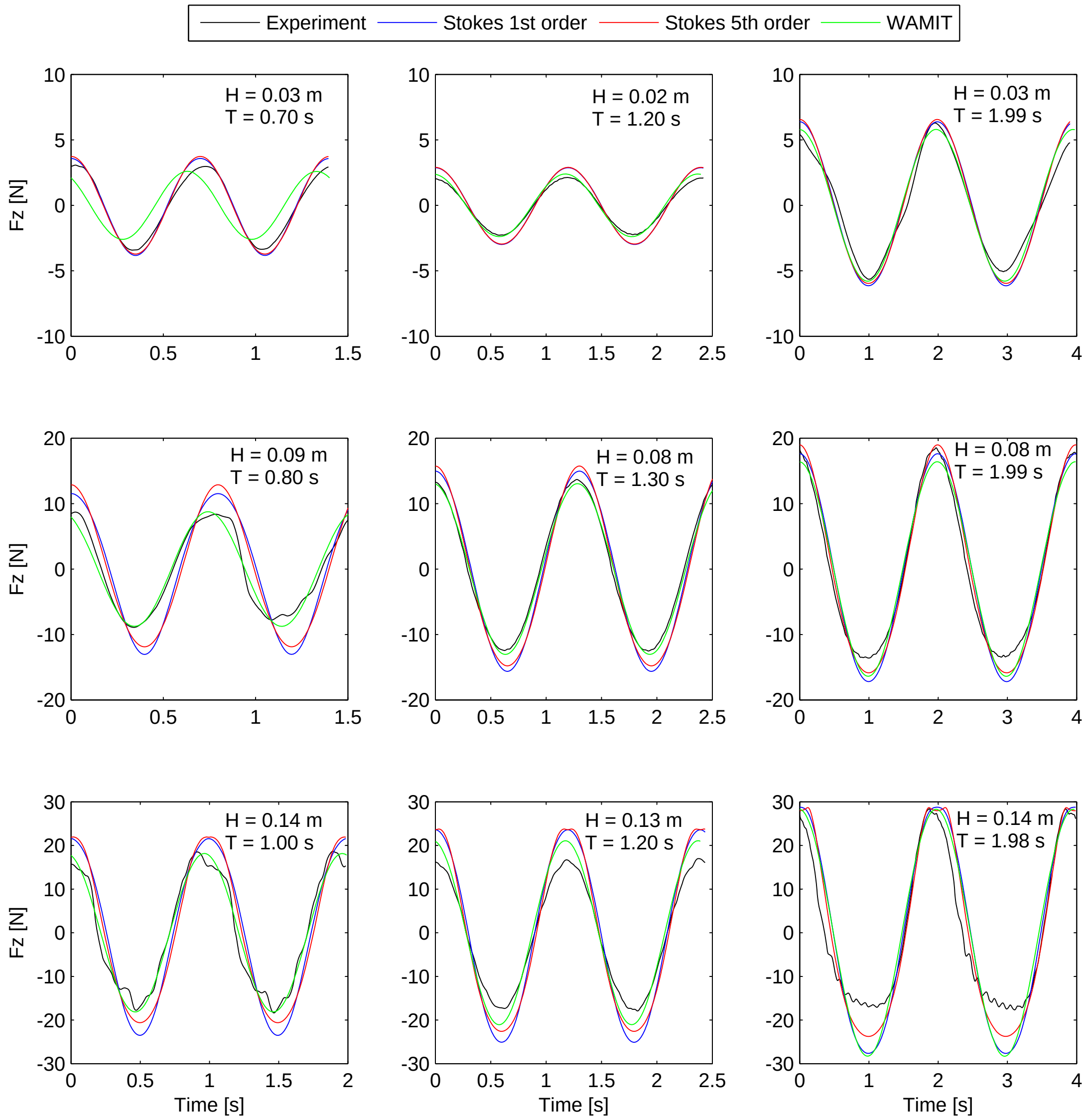

Figure I.1: Timeseries of Fz of the chosen test data compared to WAMIT and the undisturbed wave field program.

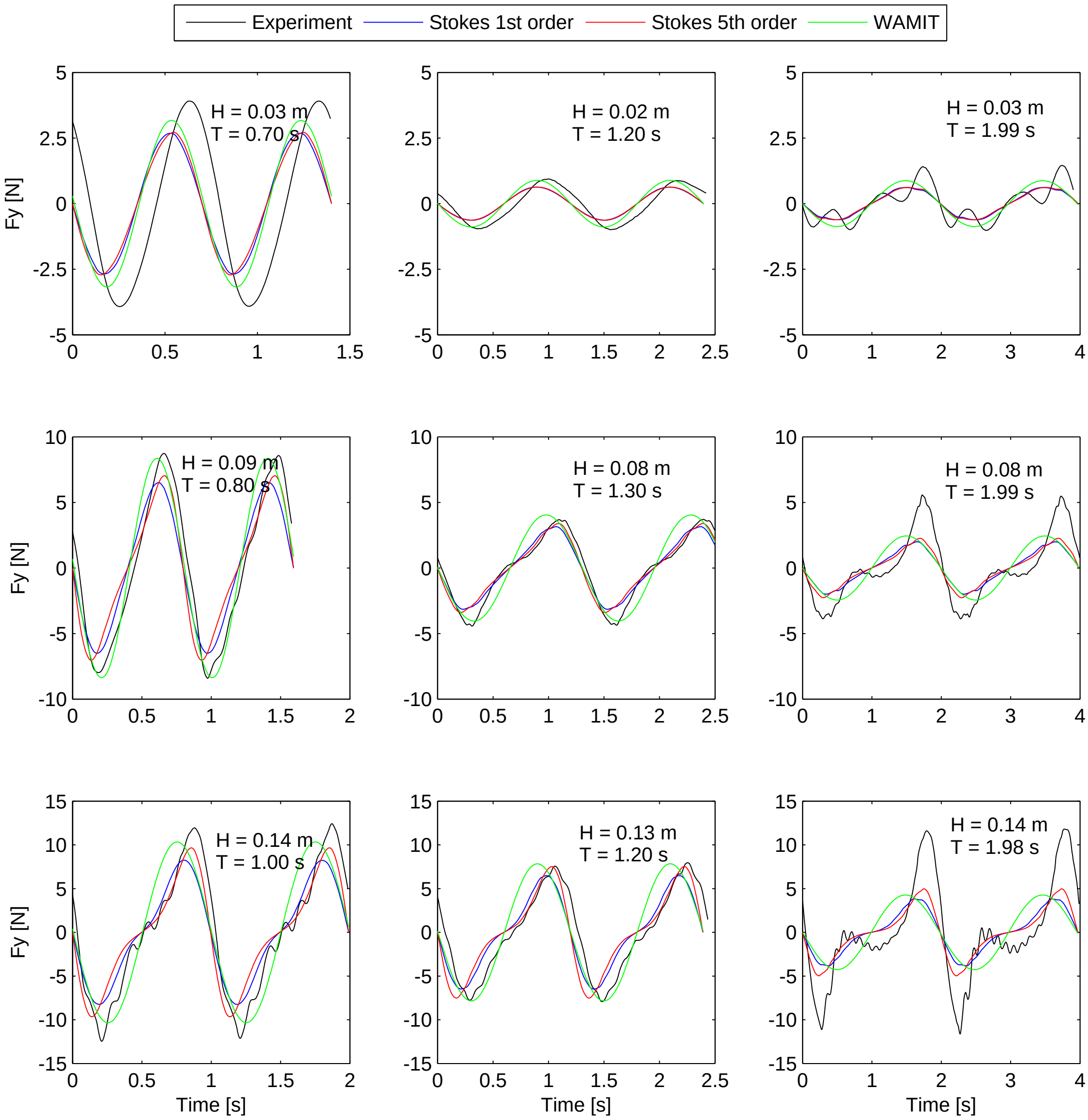

Figure I.2: Timeseries of Fy of the chosen test data comparred to WAMIT and the undisturbed wave field program.

A factor C_m is calculated between the maximum force meassured in the experiment and the maximum force calculated from WAMIT or the undisturbed wave field program using Stokes 1st order or 5th order theory, and the factors are listed in the same table overview as the test numbers.

The C_m coefficients using Stokes 1st order theory are found both without changing water level as in WAMIT and with changing water level.

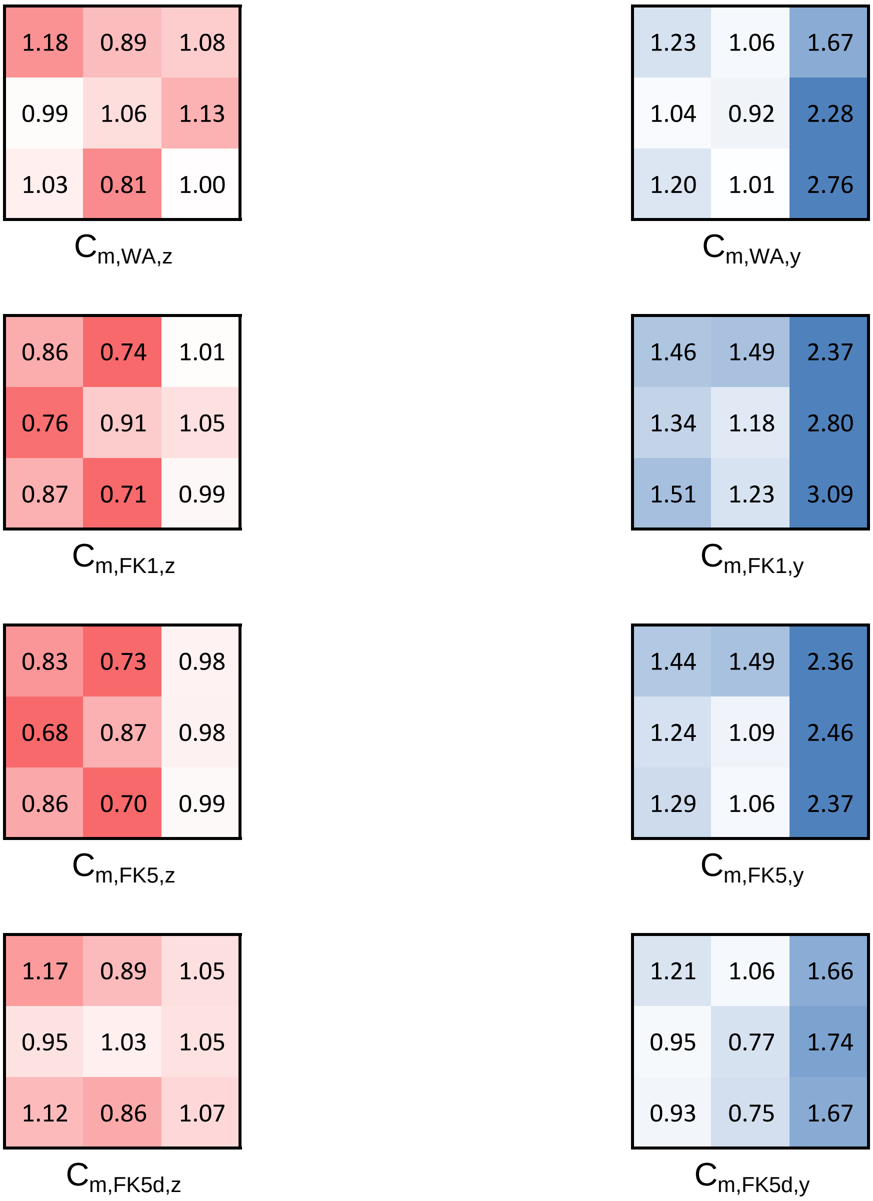

Figure I.3: C_m values.

Bibliography

WAMIT, **2006**. WAMIT. *WAMIT User Manual versions 6.4, 6.4PC, 6.3S, 6.3S-PC*, WAMIT Inc. and Massachusetts Institute of Technology, 2006.